CHAPTER TWO

PELITIC ROCKS

2.1 INTRODUCTION

Within the southern part of the New England Fold Belt, contact-metamorphosed rocks of pelitic and semi-pelitic composition are best developed around the Walcha Road Adamellite (Fig. 1). These rocks occur as a sequence of interlayered pelitic and quartzo-feldspathic units, varying in thickness from fine laminations of a few millimetres to beds over a metre wide. Korsch (1977) included these sediments in the southern part of his Sandon Association.

This study is based on samples taken from three major localities within the aureole of the Walcha Road Adamellite (Fig. 2-1 and Figs. 2-1A, B,C). This aureole is approximately 4 km wide, and four metamorphic zones have been recognised within it on the basis of mineralogical changes in pelitic rocks. The pelites show textural changes throughout the aureole, with the development of a marked foliation parallel to the contact, within the inner zones. The presence of a foliation is uncharacteristic of contact-metamorphosed pelitic sediments, and may be closely related to the emplacement mechanism of the Walcha Road Adamellite.

2.2 GEOCHEMISTRY

Analyses of four cordierite-bearing samples from the Walcha Road aureole (and one from the contact of the Mt Duval Adamellite) are shown in Table 2.1. Their variation in composition reflects the inhomogeneous layering in the original rocks. Sample 26213 is pelitic in composition, being very similar to analyses of pelites presented by other authors (e.g. Atherton, 1968; Vallance, 1960). The other samples are semi-pelitic, being mixtures, in varying proportions, of pelitic and quartzo-feldspathic material. Regardless of this chemical variation, these rocks contain a uniform mineral assemblage characteristic of pelitic hornfelses. The chemical variation in these rocks is unrelated to their distance from the pluton. Therefore, systematic changes across the aureole in both paragenesis and mineral chemistry are believed to be related to increasing metamorphic

Figure 2-1: The location of areas studied around the Walcha Road Adamellite. The geology is from Flood (1971). The grid corresponds to that on the New South Wales 1:31680 topographic sheets.

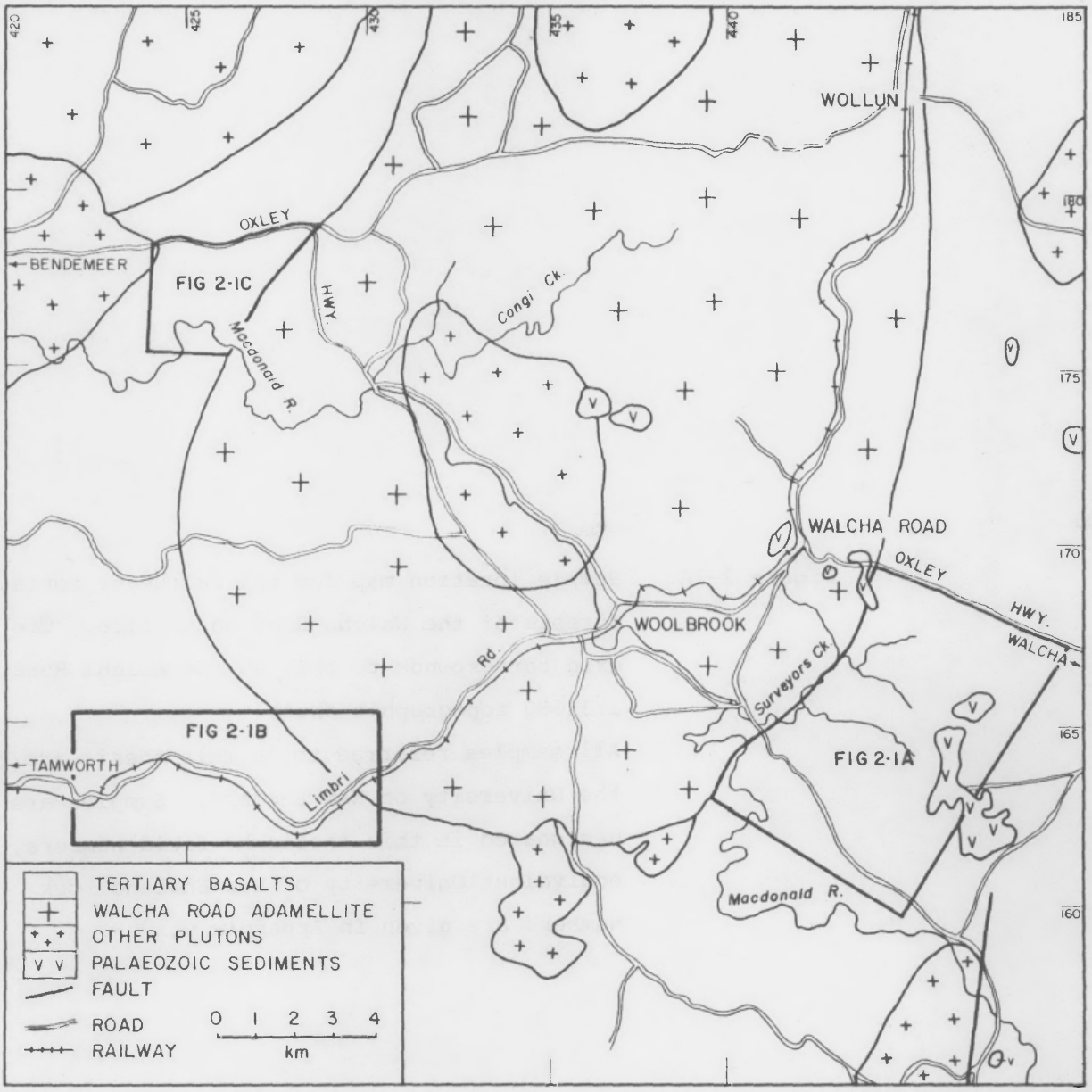
420
425
430
435
440
185
180
175
170
165
160
WOLLUN
OXLEY
BENDEMEER
FIG 2-1C
HWY.
Macdonald R.
Congi Ck.
WALCHA ROAD
OXLEY
HWY.
WALCHA
WOOLBROOK
Rd.
Surveyors Ck.
FIG 2-1B
TAMWORTH
Limbri
FIG 2-1A
Macdonald R.
TERTIARY BASALTS
WALCHA ROAD ADAMELLITE
OTHER PLUTONS
PALAEOZOIC SEDIMENTS
FAULT
ROAD
RAILWAY
0 1 2 3 4
km

Figure 2-1A: Sample location map for the southeast contact aureole of the Walcha Road Adamellite. The grid corresponds to that on the Walcha Road 1:31680 topographic sheet.
All samples referred to in this thesis are held at the University of New England. Samples are designated in this thesis by field numbers, and equivalent University of New England rock numbers are given in Appendix V.

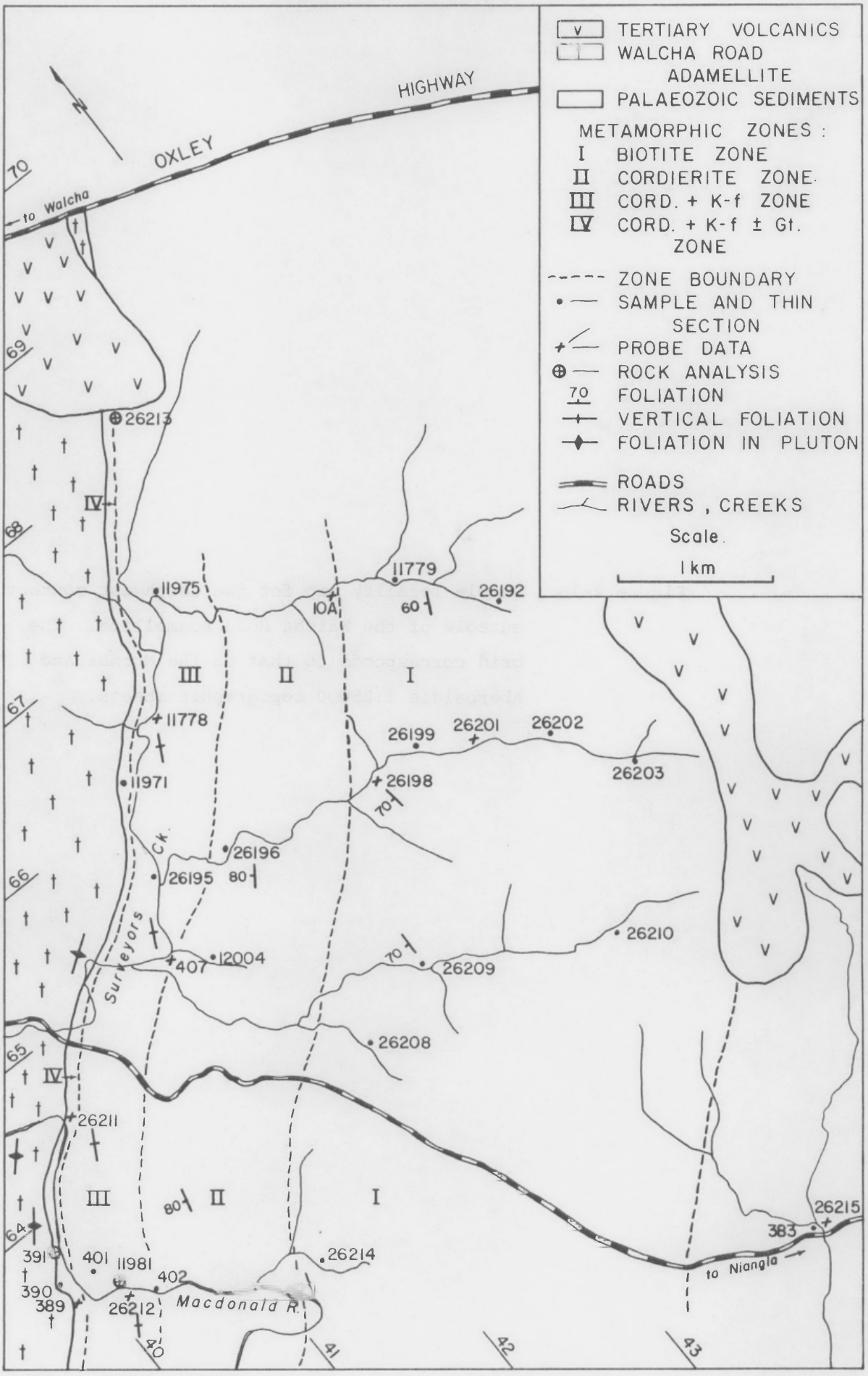
V TERTIARY VOLCANICS
WALCHA ROAD ADAMELLITE
PALAEOZOIC SEDIMENTS
METAMORPHIC ZONES :
I BIOTITE ZONE
II CORDIERITE ZONE
III CORD. + K-f ZONE
IV CORD. + K-f ± Gt. ZONE
ZONE BOUNDARY
SAMPLE AND THIN SECTION
PROBE DATA
ROCK ANALYSIS
70 FOLIATION
VERTICAL FOLIATION
FOLIATION IN PLUTON
ROADS
RIVERS , CREEKS
Scale.
1 km
HIGHWAY
OXLEY
to Walcha
to Niangla
Macdonald R.
Surveyors Ck
26213
11975
10A
11779
26192
60
11778
11971
26199
26201
26202
26203
26198
70
26196
26195
80
12004
407
26209
26210
26208
26211
26214
26215
383
391
401
11981
402
390
389
26212
80
41
42
43

Figure 2-1B: Sample locality map for the southwest contact aureole of the Walcha Road Adamellite. The grid corresponds to that on the Moonbi and Aberbaldie 1:25000 topographic sheets.

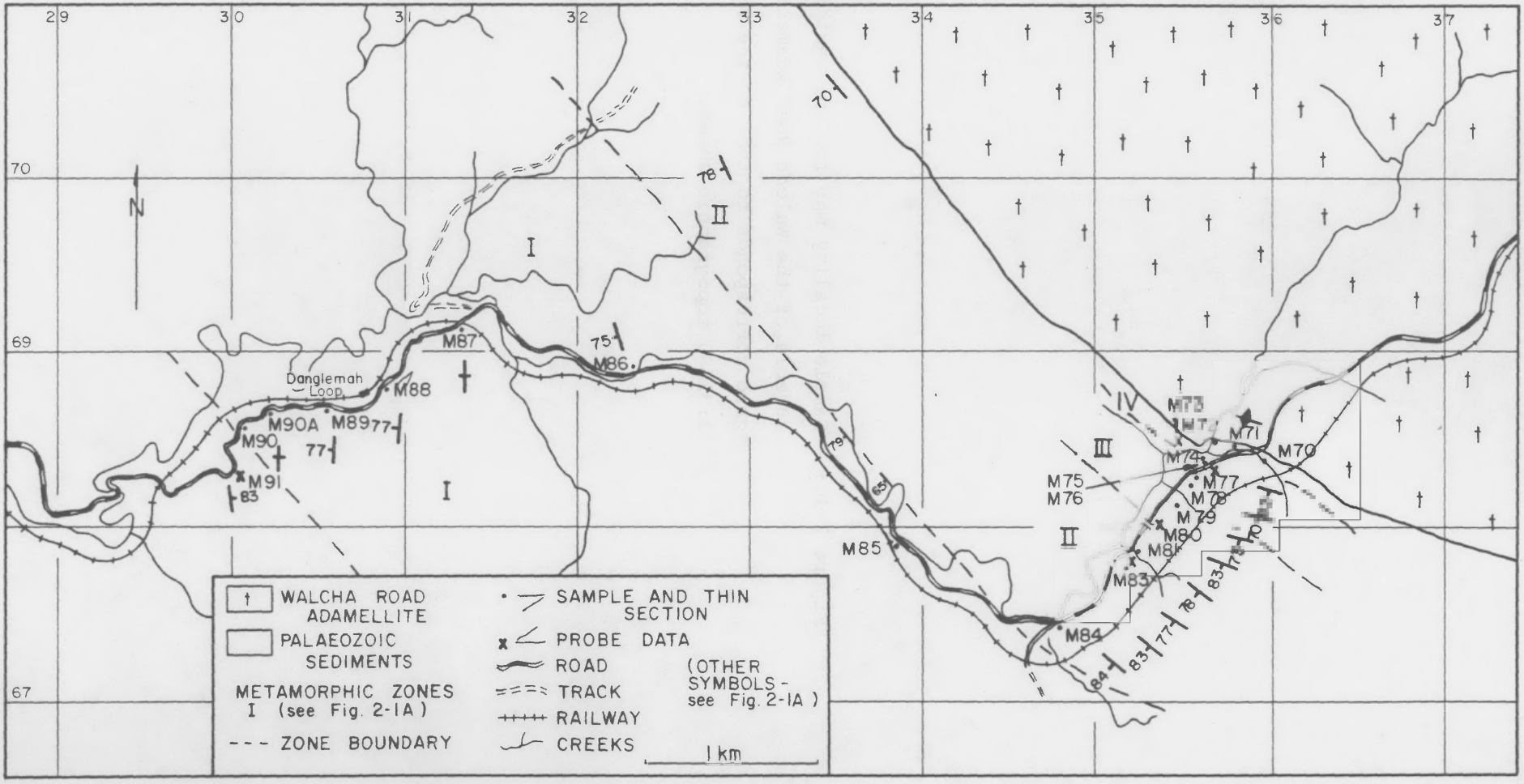
29
30
31
32
33
34
35
36
37
70
69
67
N
I
II
III
IV
M87
M86
M88
M90A
M89
M90
M91
M85
M84
M83
M82
M81
M80
M79
M78
M77
M76
M75
M74
M73
M72
M71
M70
Danglemah Loop
WALCHA ROAD ADAMELLITE
PALAEOZOIC SEDIMENTS
METAMORPHIC ZONES I (see Fig. 2-1A)
ZONE BOUNDARY
SAMPLE AND THIN SECTION
PROBE DATA
ROAD
TRACK
RAILWAY
CREEKS
(OTHER SYMBOLS - see Fig. 2-1A)
1 km

Figure 2-1C: Sample locality map for the western contact aureole of the Walcha Road Adamellite. The grid corresponds to that on the Bendemeer 1:31680 topographic sheet.

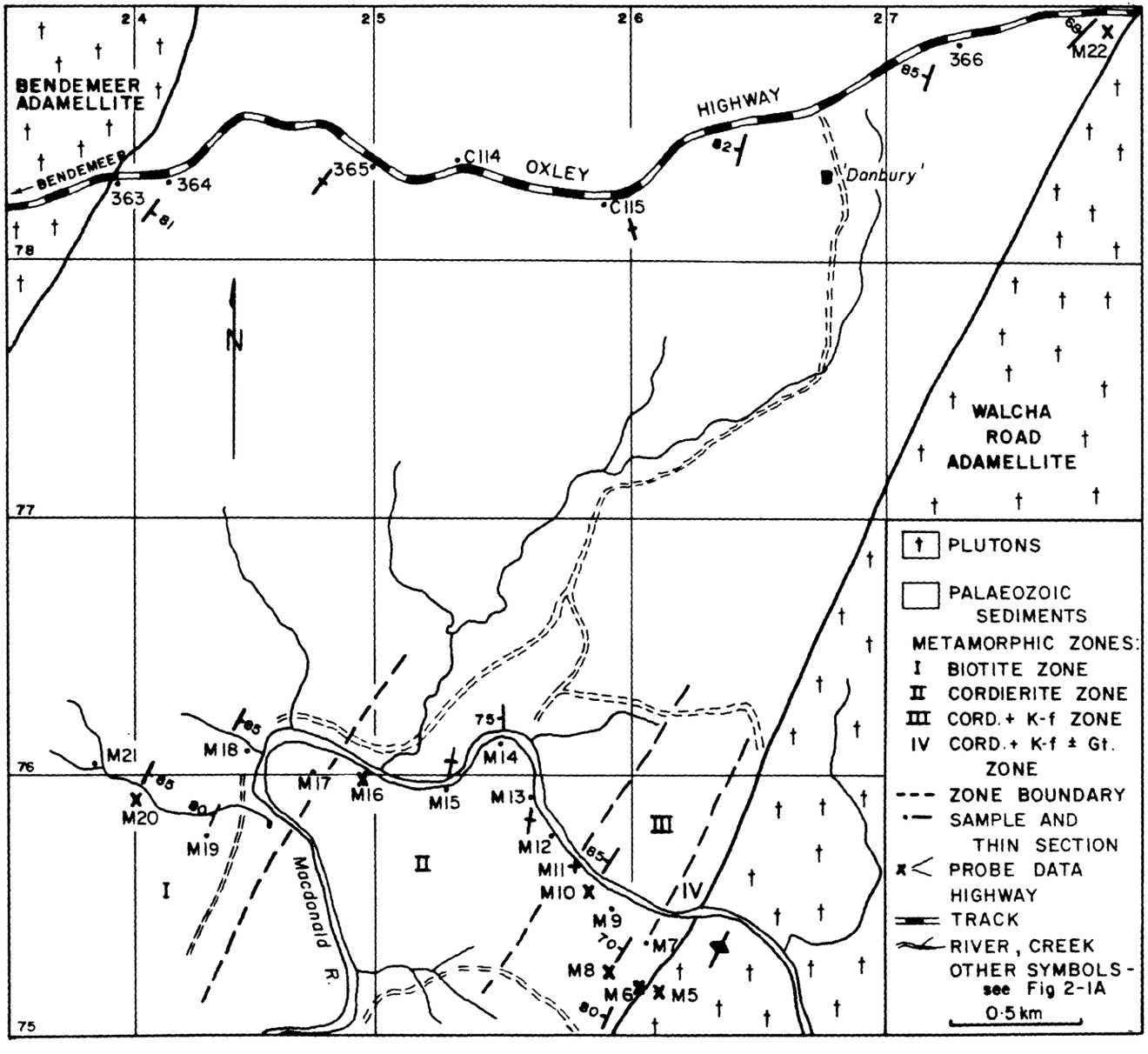
BENDEMEER ADAMELLITE
BENDEMEER
363
364
365
C114
OXLEY
C115
HIGHWAY
'Danbury'
366
M22
WALCHA ROAD ADAMELLITE
M21
M18
M17
M16
M15
M14
M13
M12
M11
M10
M9
M8
M7
M6
M5
M20
M19
Macdonald R.
I
II
III
IV
N
PLUTONS
PALAEOZOIC SEDIMENTS
METAMORPHIC ZONES:
I BIOTITE ZONE
II CORDIERITE ZONE
III CORD.+ K-f ZONE
IV CORD.+ K-f ± Gt. ZONE
ZONE BOUNDARY
SAMPLE AND THIN SECTION
PROBE DATA
HIGHWAY
TRACK
RIVER, CREEK
OTHER SYMBOLS - see Fig 2-1A
0·5 km

TABLE 2.1. Chemical analyses of contact-metamorphosed pelitic and semi-pelitic sediments

Sample No.	391*	64	26213	11981	11985
Distance†	0	10m	100m	300m	1100m
SiO_2	62.56	68.15	54.79	71.37	65.72
TiO_2	0.80	0.58	1.10	0.68	0.96
Al_2O_3	17.40	14.65	22.20	12.89	15.48
Fe_2O_3	1.54	0.88	1.83	1.13	1.00
FeO	3.81	3.71	6.46	4.13	4.77
MnO	0.16	0.14	0.09	0.13	0.10
MgO	2.20	1.25	2.92	1.79	2.10
CaO	2.72	1.05	0.88	1.49	2.50
Na_2O	3.70	1.57	1.58	2.50	3.46
K_2O	3.45	4.65	5.60	2.27	2.31
P_2O_5	0.23	0.12	0.13	0.11	0.18
H_2O^+	1.20	1.70	1.87	1.12	1.21
H_2O^-	0.15	0.62	0.50	0.28	0.16
Insoluble Residue	0.08	0.50	0.05	0.10	0.05
Total	100.00	99.57	100.00	100.00	100.00
Trace elements (ppm)					
Rb	83	214	134	67	59
Sr	363	137	136	188	294
Y	42	31	45	26	46
Zr	207	138	192	111	139
Nb	8	12	20	8	8
MgO/MgO+FeO	0.366	0.252	0.311	0.302	0.306

† Distance from the igneous contact

* Sample of migmatite

Sample 64 is from the aureole of the Mt Duval Adamellite. The other samples are from the Walcha Road Adamellite aureole.

Analyses by R.H. Roberts and G.I. Kolocsai: samples 391, 26213, 11981 and 11985 were analysed by wet chemistry (SiO_2 by difference), sample 64 by XRF except Na_2O, FeO, H_2O^+ and H_2O^-.

grade rather than to metasomatism or variation in whole-rock composition.

2.3 PETROGRAPHY OUTSIDE THE AUREOLE

Pelitic sediments outside the aureole have been regionally metamorphosed to low-grade slates with a slaty cleavage parallel to bedding. The slates and slaty bands in the layered rocks are characterised by a grey-green colour, though, a reddish appearance often results from weathering. The pelitic (slaty) material consists predominantly of fine-grained quartz, plagioclase, K-feldspar, sericite, chlorite, graphite, and opaques. Alignment of sericite and chlorite defines the slaty cleavage. In more-weathered samples the chlorite is replaced by a brownish material (vermiculite?), discussed in Chapter Three, Section 3.3. Siltsize grains of quartz and opaques (some displaying the reddish colour of hematite) are prominent throughout the finer material, and are commonly elongated parallel to the general fabric. The opaque grains are typically associated with an orange-brown alteration product. The felsic layers within these sediments consist predominantly of quartz, feldspar, and fine sericite. These rocks also show deformational features such as buckling within the laminated sediments and boudinage in the more coarsely layered samples.

2.4 PETROGRAPHY OF THE CONTACT METAMORPHOSED ROCKS

2.4.1 Introduction

Because of their very fine grainsize, precise modal analyses of the pelitic hornfelses are not practicable. Therefore, the broader modal variations are presented only qualitatively in Fig. 2-2. This Figure is based mainly on the pelitic portions of the rocks, ignoring the more obvious quartzo-feldspathic layers. From these data, four mineralogical zones have been recognised within the pelitic sediments of the Walcha Road aureole (as shown in Fig. 2-2). These are (with distances from the contact given in brackets):

I) Biotite zone (4 km - 1500 m);
II) Cordierite zone (1500 m - 500 m);
III) Cordierite + K-feldspar zone (500 m - 100 m);
IV) Cordierite + K-feldspar ± Garnet zone (100 m - contact).

Figure 2-2: Schematic representation of the variation in modal composition of pelitic hornfelses with increasing grade (distance from the contact) in the aureole of the Walcha Road Adamellite. Garnet is not ubiquitous in the cordierite + K-feldspar ± garnet zone.

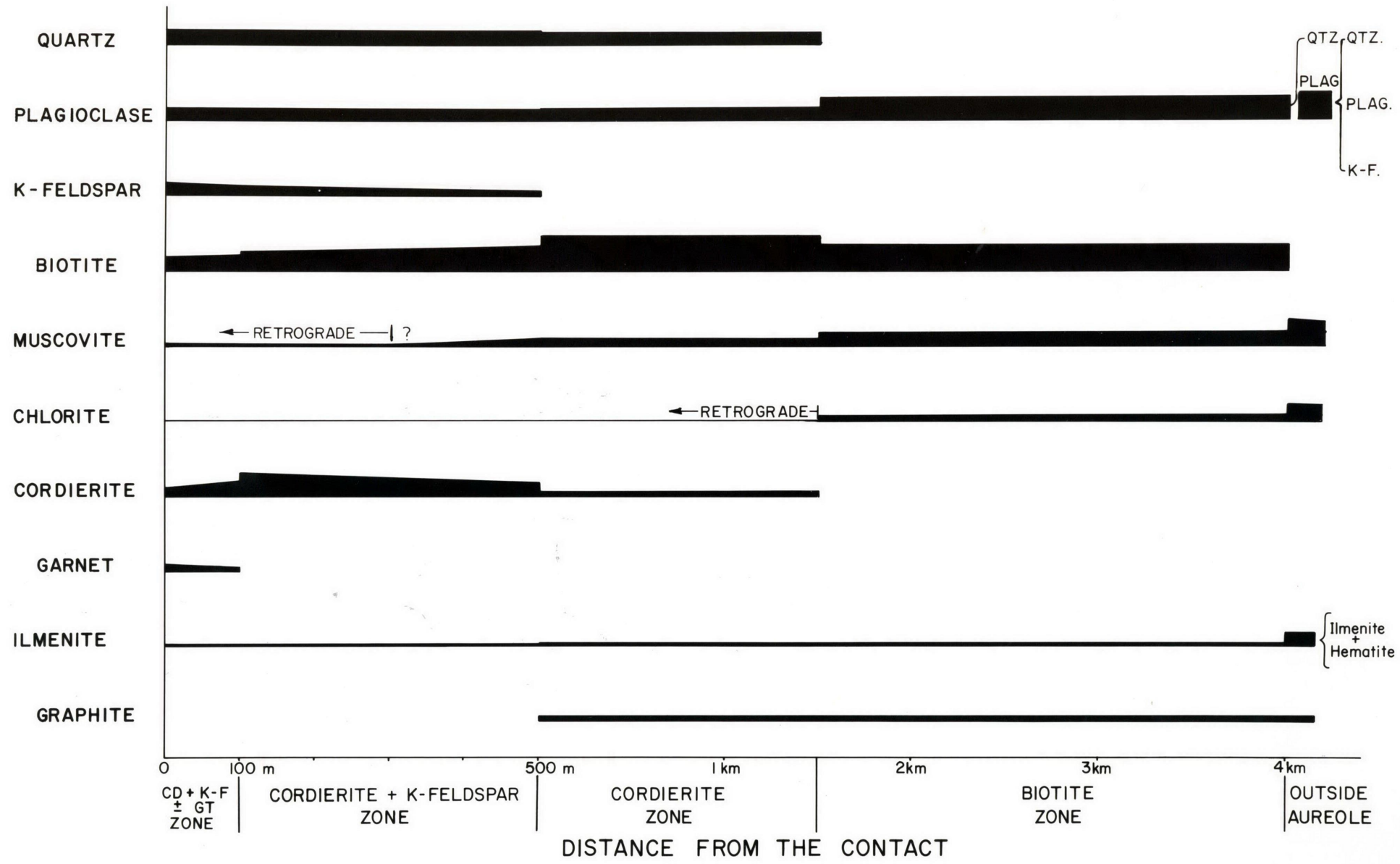
QUARTZ
PLAGIOCLASE
K-FELDSPAR
BIOTITE
MUSCOVITE
CHLORITE
CORDIERITE
GARNET
ILMENITE
GRAPHITE
QTZ
QTZ.
PLAG
PLAG.
K-F.
RETROGRADE ?
RETROGRADE
Ilmenite + Hematite
0
100 m
500 m
1 km
2km
3km
4km
CD + K-F ± GT ZONE
CORDIERITE + K-FELDSPAR ZONE
CORDIERITE ZONE
BIOTITE ZONE
OUTSIDE AUREOLE
DISTANCE FROM THE CONTACT

These zones are shown for the different traverses in Figs. 2-1A,B and C.

2.4.2 Biotite Zone

The outer limit of this zone is marked by the abrupt appearance of ubiquitous brown biotite. This gives the rock a characteristic black colour, which is distinct from the greener colour of the regionally metamorphosed slates. Green biotite has been noted in some thin sections of the slates immediately on the low-grade side of this boundary. However, it is typically poorly developed and occurs only sporadically within veins; it is therefore considered impracticable as a zone indicator.

Throughout the biotite zone the rocks consist mainly of quartz, plagioclase, biotite, sericite, chlorite, opaques, and abundant stringers and lenses of graphite. Compositional layering, typical of the original slates, continues to be prominent and, although slightly diminished, a well developed cleavage is still obvious and the rocks retain much of their slaty appearance. The cleavage continues to be defined by preferred orientation of the chlorite and sericite. The newly developed biotite typically lacks a preferred orientation, occurring as small (less than 0.01 mm) randomly orientated flakes (Plate 2-1A). Conversely, some biotite can be aligned with the chlorite and sericite, possibly mimicking the slaty cleavage or resulting from the impingement of grain growth (Spry, 1974).

Chlorite in this zone typically occurs as fine grains or stringers. However, occasional coarser flakes of chlorite cut randomly across and enclose the earlier fabric. This fabric, including stringers of graphite, appears to pass undisturbed through the flakes (Plate 2-1B). Cross-cutting chlorite flakes have been described in other studies of low-grade pelitic rocks (e.g. Compton, 1960; Hollister, 1969; Novak and Holdaway, 1981), and Novak and Holdaway (1981) have suggested that the chlorite flakes described by them are pseudomorphs after staurolite. No evidence of such an origin was found in this study.

2.4.3 Cordierite Zone

This zone is characterised by the appearance of cordierite porphyroblasts. With the incoming of cordierite, chlorite and muscovite no longer coexist. Typically (though not exclusively, e.g. sample M82)

PLATE 2-1: Textures in pelites from the outer zones of the Walcha Road Adamellite aureole. All photomicrographs taken under plane-polarized light.

A: Randomly orientated flakes (sample M18; biotite zone). Width of photograph covers 0.55 mm.

B: Three coarse rectangular flakes of chlorite cut across the earlier fabric (sample M21; biotite zone). The earlier fabric (including graphite stringers) passes undisturbed through the two larger flakes slightly southeast and north of centre. The third flake occurs in the southwest corner of the photograph. Width of photograph covers 0.55 mm.

C and D: A cordierite porphyroblast from the extreme outer part of the cordierite zone (sample M16). The cordierite shows no preferred orientation and no foliation is apparent in the biotite-rich groundmass. Width of photograph C covers 1.40 mm width of photograph D covers 0.55 mm.

E and F: Biotite foliation from the cordierite zone (sample 12004). An elongated cordierite porphyroblast is partially shown in the lower half of photograph E. Width of photograph E covers 1.40 mm, width of photograph F covers 0.55 mm.

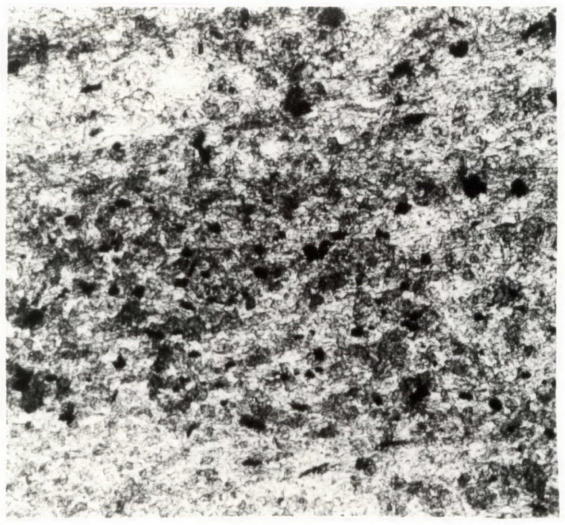

A

B

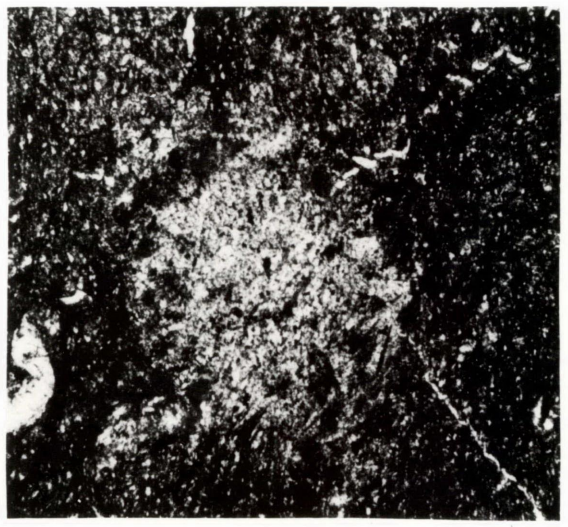

C

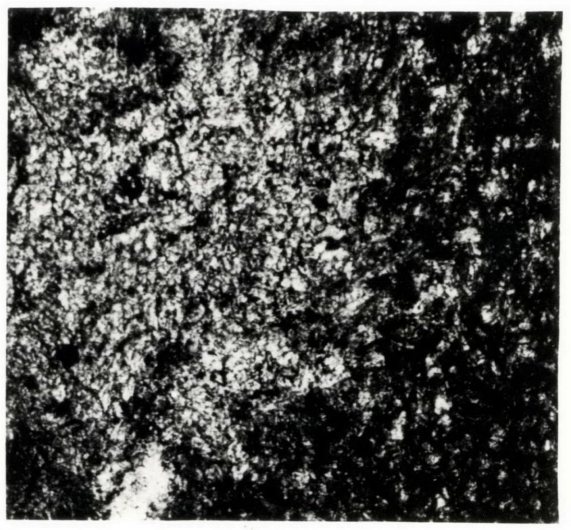

D

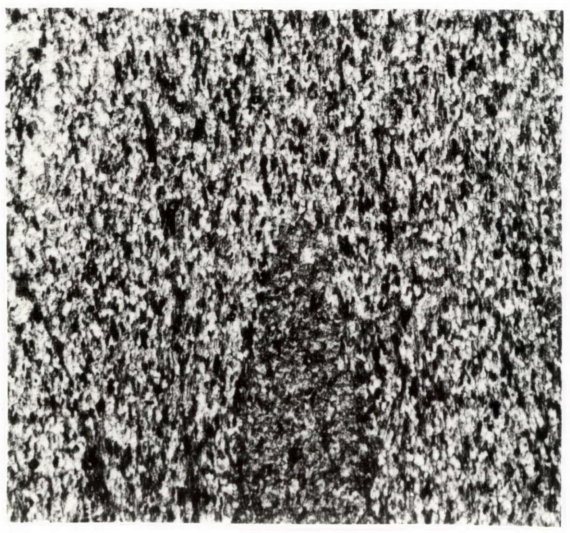

E

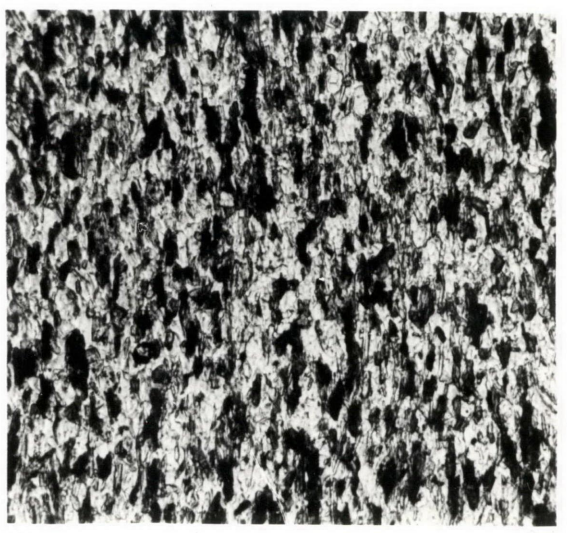

F

chlorite is the phase lost, resulting in a fine-grained assemblage of quartz, plagioclase, sericite, biotite, cordierite and opaques (fibrous clusters of retrograde chlorite, however, are commonly present from the breakdown of cordierite). The incoming of cordierite appears to be associated with a general increase in the biotite content. The outer cordierite-zone boundary is not marked by a significant difference in the appearance of the hand specimen, except that some samples are distinctly spotted. These spots are discussed below.

Texturally, this zone is characterised by a further increase in grainsize and the formation of a biotite-rich fabric. The original slaty cleavage, defined by chlorite and sericite, is no longer evident within this zone, due to the major decrease in these phases at the cordierite isograd. In the extreme outer part of this zone the rocks characteristically lack a well defined foliation. In thin section the biotite occurs as randomly orientated flakes, while the cordierite has round-to-oval-shaped cross-sections with no apparent preferred elongation (e.g. sample M16, Plate 2-1C and D). As the contact is approached a foliation defined by biotite is developed. This biotite foliation continues to develop with increasing grade, and the cordierite porphyroblasts commonly become elongated in the direction of this foliation (Plate 2-1E and F). The biotite foliation both abuts against and bends around the porphyroblasts. (This texture is more apparent in the cordierite + K-feldspar zone, as described in Section 2.4.4). Grainsize also continues to increase with increasing grade and the highest-grade rocks of this zone have a distinctly phyllitic appearance.

Within this zone the biotite foliation commonly cuts across the bedding (e.g. M15,M83), whereas at lower grade the slaty cleavage and bedding are apparently parallel. This implies that the biotite defines a new foliation distinct from the earlier slaty cleavage (however, it remains a possibility that the slaty cleavage was originally oblique to bedding in these specific examples). The biotite foliation broadly parallels the pluton contact, and can be considered to be "granite-induced" (as described by Pitcher and Read, 1963, around the Ardura Pluton). Further evidence for a granite-induced origin of this foliation has been discussed in Section 1.6.3.

Many examples occur in this zone of small-scale folding (exemplified

by tightly folded felsic veins, e.g. samples M84B,M12) with the presumedly granite-induced foliation parallel to the axial planes. Therefore, it is likely that these folds also owe their origin to the emplacement of the pluton. No evidence exists in these rocks of crenulation of the previous slaty cleavage, as the earlier chlorite + sericite fabric is no longer prominent (noted above). White mica which remains in these rocks is exceptionally fine grained and its orientation is difficult to ascertain. Coarse plates of muscovite occur both aligned with, and randomly cutting across, the biotite foliation.

Rocks in the extreme outer part of this zone lack a foliation, probably because contact metamorphism (causing the breakdown of chlorite and sericite) has obliterated the slaty cleavage without, unlike the rest of the cordierite zone, the development of a biotite fabric caused by directed pressures associated with the pluton's emplacement.

The cordierite in the rocks studied is commonly altered to a retrograde assemblage of sericite, chlorite and opaque oxides. Also associated with the alteration of cordierite, especially around its edges, is an amorphous isotropic yellow material. This has been analysed and is discussed further in Section 2.5.6. Commonly, patches of this yellow material, or clusters of chlorite are the only remaining evidence of previous cordierite.

In the outer part of the zone, some samples (e.g. 342A) contain dark spots. Although obvious in hand specimen, in thin section these spots can be difficult to discern from their surrounding matrix. However, they can be distinguished by their finer grainsize, the lack of preferred orientation of their internal constituents, and deflection of the biotite fabric around them. The spots consist mainly of fine-grained muscovite, quartz, plagioclase, minor biotite, a few opaque grains, and small clusters of chlorite. Although noted repeatedly within the outer zones of contact aureoles, the origin of these spots is still questionable. The spots described here are thought to represent cordierite porphyroblasts, for their outlines are texturally identical to more obvious cordierites of this zone. Harker (1974) and Tilley (1923) believed that spots of this sort could represent the embryonic formation of porphyroblasts (though the material described by Harker (1974) appears to be the yellow alteration product mentioned above). Alternatively, they may be of retrograde origin,

with their indistinct appearance in thin section, relative to the matrix, being due to the alteration of cordierite sieved with a large amount of matrix material.

2.4.4 Cordierite + K-feldspar Zone

This zone is marked by the incoming of K-feldspar and a major increase in cordierite (Fig. 2-2). This is associated with a sharp decrease in muscovite content and, to a less obvious degree, in biotite; muscovite is commonly absent from the rocks of this zone, whereas biotite continues to be a major phase. The boundary is further delineated by the loss of graphite, which gives the rocks a distinctly lighter colour. The usual assemblage in the cordierite + K-feldspar zone is therefore quartz, plagioclase, K-feldspar, cordierite, biotite and opaques, with or without muscovite. With increasing grade across this zone, there is an overall increase in cordierite and K-feldspar, and a decrease in biotite.

The rocks are coarser grained than in the cordierite zone and have undergone major textural reconstitution to a strongly recrystallised polygonal texture (i.e. dominated by straight boundaries and triple points), within which a prominent foliation (schistosity) is defined by the alignment of biotite. The more-pelitic rocks of this zone possess a major biotite foliation and can be appropriately referred to as schists. Bedding is still recognisable within the rocks as compositional layering, and both bedding and foliation generally parallel the perimeter of the pluton.

The cordierite and K-feldspar occur as porphyroblasts. The cordierites are characteristically large (3-4 mm), and sieved with non-aligned inclusions of quartz, plagioclase, K-feldspar, biotite and opaque grains. Cordierite alteration is the same as in the cordierite zone, involving replacement by fine sericite, chlorite, and opaque grains. The yellow isotropic alteration product is again common and is especially obvious around the borders of otherwise fresh cordierites. K-feldspar porphyroblasts are smaller (<1 mm) and less easily identified. They are also sieved and typically display a grey alteration product of possibly sericite or clay.

The biotite foliation is deflected around the cordierite porphyroblasts, and in some rocks the schistosity can appear quite anastomosing

Plate 2-2: Textures in pelites from the inner zones of the Walcha Road Adamellite aureole. All photomicrographs taken under plane-polarized light.

A: Biotite foliation both wraps around and abutts against the cordierite porphyroblasts from the cordierite + K-feldspar zone (sample 2621 2). Width of photograph covers 2.25 mm.

B: An enlargement of the texture around the lower half of the central cordierite porphyroblast in photograph A. Width of photograph covers 0.90 mm.

C: Thin gneissic banding from the cordierite + K-feldspar ± garnet zone (sample M71). The felsic layers consist of quartz, K-feldspar and plagioclase, whereas the mafic layers are rich in biotite. Width of photograph covers 2.25 mm.

D: A felsic vein (right-hand side of photograph) in sample 391 - a sample of migmatite. The felsic vein consists of quartz, K-feldspar, plagioclase and minor biotite. Alteration of K-feldspar to sericite is evident in the photograph (darker fibrous material). The host rock (left-hand side of photograph) is rich in biotite. A selvedge of coarse-grained biotite lies along the border of the felsic vein. Width of photograph covers 2.25 mm.

A

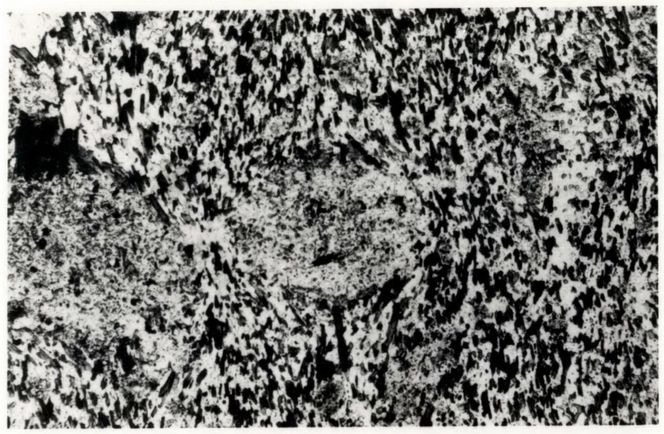

B

C

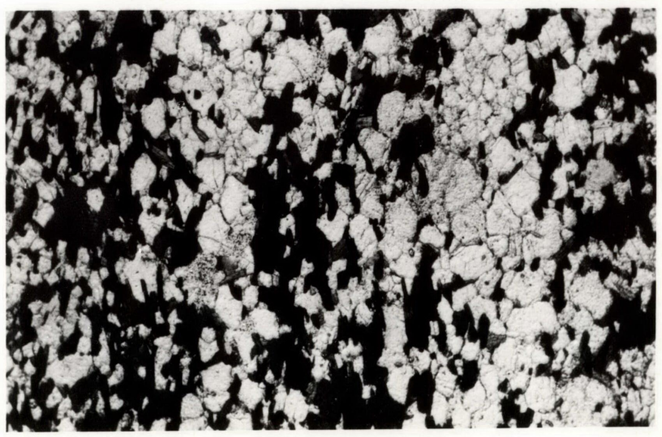

D

because of the abundance of porphyroblasts within them. However, in detail, the biotites also abut against the cordierite porphyroblasts (Plate 2-2A and B). Interpretation of this textural relationship is ambiguous. It is possible the cordierite has grown across a previous biotite foliation, followed by a deformation which has moulded the biotite around the porphyroblasts. Such a history seems unnecessarily complex for these rocks. Saggerson (1974) described similar textures within a contact aureole and interpreted them to unequivocally show the displacement of "S"-surfaces by the porphyroblast's growth. However, Vernon and Powell (1976) have argued against this interpretation, and suggested that as little as 1% bulk strain imposed externally on the rocks could develop these textures. They also point out that the order of crystallisation is often unrecognisable on the basis of moulding and inclusion relationships, and suggest that such relationships can be associated with the simultaneous growth of the phases involved. The simplest interpretation for the cordierite-biotite relationships in these rocks is therefore believed to involve the simultaneous growth of the two phases, with the biotite deflecting around the porphyroblasts due to the stress associated with the emplacement of the pluton. Similar textures occur around the K-feldspar porphyroblasts, but they are less apparent because of the smaller size of these porphyroblasts.

Muscovite is commonly absent from the cordierite + K-feldspar zone, as noted above, but it does occur as a major constituent of the prograde assemblage in some rocks in the outer 50m of the zone (e.g. M80). Muscovite occurs at higher grades within this zone, but most of this is clearly retrograde after cordierite. However, one sample (M78) at 250m from the contact, contains abundant muscovite plates apparently unrelated to the cordierite alteration. These plates commonly cut across the biotite foliation, and although this could imply formation after the biotite (retrograde muscovite), Evans and Guidotti (1966) stated that this need not be so. Textural evidence for the origin of muscovite in this sample is therefore ambiguous. Further discussion of the muscovite in sample M78 is given in Section 2.7.3.

2.4.5 Cordierite + K-feldspar ± Garnet Zone

Although the presence of garnet is characteristic of this zone, its occurrence is strongly dependent on composition (discussed in Section

2.7.3), and therefore does not define a sharp isograd. In the absence of garnet, the mineral assemblage remains the same as in the higher-grade part of the cordierite + K-feldspar zone (i.e. quartz + plagioclase + K-feldspar + cordierite + biotite and opaque oxide). The incoming of garnet is not associated with the diagnostic loss of any phase, although it coincides with a decrease in both biotite and cordierite, and an increase in K-feldspar (Fig. 2-2). Garnet occasionally occurs without cordierite, and in one sample (349) garnet exists in a quartzo-feldspathic assemblage, with only minor biotite. Biotite-containing assemblages with neither cordierite nor garnet also occur throughout the zone and are believed to represent more-felsic original layers.

Owing to the non-definitive nature of the garnet paragenesis, the outer limit of the zone can be only approximately placed at 100 metres from the contact. At this distance distinct textural changes are noted. In hand specimen the rocks tend to lose their strong schistosity, owing to their decrease in biotite content, and develop a distinctive thin gneissic banding (Plate 2-2C). Grainsize has increased to between 0.2 and 0.5 mm, and the rocks are totally recrystallised, with the biotite occurring as well aligned flakes within a granoblastic-polygonal aggregate of quartz and feldspar. Cordierites in these rocks do not occur as sieved oval-shaped porphyroblasts, as in the previous zones, but as inclusion-free rectangular grains of higher relief (greater than quartz). This change in appearance of the cordierite can not be related to any obvious compositional differences. Garnet occurs as large equidimensional porphyroblasts containing minor inclusions of quartz. The garnet typically cuts across the biotite foliation, though, some samples show minor deflection of the biotite fabric around them.

Retrograde muscovite occurs in this zone both as fine-grained aggregates and as large plates. The coarser muscovite commonly appears as pseudomorphs after biotite, leaving the biotite as relict poorly defined grains. This muscovite typically replaces biotite in contact with cordierite, suggesting a retrograde breakdown involving these two minerals (see Section 2.6.6). Fine muscovite replaces K-feldspar, and is also commonly associated with chlorite in felty aggregates replacing cordierite. The chlorite is not always obvious, but the muscovite usually has a distinctive greenish colour and lower-than-normal birefringence (up to first-order orange and yellow interference colours), believed to represent a fine intergrowth of the two minerals. Chloritic alteration of biotite

does occur, though it is mainly found in rocks lacking cordierite and garnet.

As mentioned above, gneissic banding parallel to the pluton contact occurs within this zone. The felsic layers consist of a granoblastic polygonal aggregate of quartz, K-feldspar and plagioclase, whereas the mafic layers contain biotite as well as these felsic phases(Plate 2-2C). Biotite is occasionally concentrated at the edges of the felsic layers as poorly developed selvedges.

Some of this layering may be a relict feature inherited from the original rocks, but its ubiquitous presence in this zone when compared to lower-grade zones, suggests a metamorphic origin. Such banding is frequently equated with metamorphic segregation (e.g. Robin, 1979, his type-L). Robin believes the felsic layers to be derived from within the host rock, by the stress-induced movement of certain elements (especially Si) into low-pressure areas. From the present study, little can be concluded about the possible role of metamorphic segregation in the formation of this layering. Much of the layering could be related to the early stages of migmatite formation (discussed in Section 2.8).

Close to the contact, steeply plunging tight to isoclinal folds commonly occur within the pelites, with their axial planes roughly parallel to the pluton perimeter (excellent examples of these folds occur at sample locality M22, a road cutting on the Oxley Highway, and sample localities M71 and M72). The folds are predominantly small scale rarely being more than a few centimetres in amplitude or wavelength and varying down to the scale of millimetres. Bedding (still identifiable by variations in grainsize and composition) has been folded, and the biotite foliation is parallel to the axial plane of these folds (M22). In sample M22 the thin gneissic layering is also parallel to the biotite foliation, and hence axial plane to the folds. This folding is believed to be related to the emplacement of the pluton, developing during the peak of metamorphism, and is equivalent to the folding described in the cordierite zone.

Quartz-rich and quartzo-feldspathic veins within the pelites have also been isoclinally folded in this event. These veins can be similar in appearance to the felsic layers of the gneissic banding (though typically coarser-grained), however, in sample M71 they are clearly distinct, with

the gneissic layering and biotite foliation occurring parallel to the axial planes of the folded veins. This veining may be inherited from the original sediments, though, it is possible that it formed during the early stages of metamorphism and has subsequently been folded as metamorphism developed.

At the contact, these earlier features of bedding and cross-cutting veins are difficult to distinguish, owing to the continued increase in grainsize and the development of a larger-scale gneissic layering that is associated with further recrystallisation and the local formation of migmatites.

2.4.6 Migmatite Outcrops

Contacts of the Walcha Road Adamellite with pelitic rocks are commonly characterised by outcrops of migmatitic appearance (e.g. sample localities 391, Fig. 2-1A; M6, Fig. 2-1C). These outcrops contain leucocratic material as intensely folded thin veins. These veins are coarser grained than their host rock, and consist of quartz, plagioclase and K-feldspar in an allotriomorphic-granular texture. Much of the coarse plagioclase lacks twinning (and was distinguished from K-feldspar only after staining with sodium cobaltnitrite). Minor well twinned plagioclase and biotite are scattered throughout the veins and tourmaline occurs sporadically. The veins are typically bordered by a zone rich in coarse biotite (Plate 2-2D). Coarse plagioclase occurs with the biotite, and where cordierite or garnet or both are present in the rock they are also concentrated along the edges of the felsic veins. Intense hydrous alteration is associated with the felsic veins, and the alteration is often exclusive to them. These features are identical to those described in migmatites by several other authors (e.g. White, 1966; Ashworth, 1976; Yardley, 1978). The origin of such features, though, is still debatable, as discussed in Section 2.8 on the genesis of the migmatites.

The migmatite outcrops are also characterised by coarse-grained (2-3 mm) quartzo-feldspathic lenses ranging up to half a metre across, which are commonly wrapped by the thinner veins. These lenses are identical in mineralogy and texture to the felsic veins. At sample locality M6 (Fig. 2-1C) there appears to be a progressive change from the veined sediments into the quartzo-feldspathic lenses, over a distance of 10-20 cm.

The change begins with a coarsening of the felsic material and a widening of the veins, which causes disruption of the general layering. With continued coarsening and concentration of the felsic material, an essentially granitic rock forms, containing only relict patches of veined sediment, which grades into the quartzo-feldspathic lenses. Therefore, it is feasible that these lenses represent accumulations of the vein material.

Medium-to fine-grained granitic dykes, texturally and mineralogically identical to the leucocratic material in the migmatites, also occur near the pluton contacts. It is tentatively suggested that these dykes could have been derived in the same manner as the veins and lenses, but have been more completely mobilised (also see Section 2.8).

2.5 MINERAL CHEMISTRY

2.5.1 Introduction

This section is concerned with the variations in mineral chemistry related to grade (distance from the contact). Obvious variations in mineral chemistry can be related directly to initial differences in the whole rock chemistry, but systematic changes between the metamorphic zones are still discernible. Discussion of these changes with respect to the postulated metamorphic reactions is given in Section 2.7.

2.5.2 Feldspars

Plagioclase compositions range from andesine to calcic oligoclase ($Ab_{60} \rightarrow Ab_{75}$). No consistent changes were noted with increasing grade, though, in garnet-containing rocks the plagioclase is significantly more sodic ($Ab_{75} \rightarrow Ab_{80}$). All K-feldspar analyses show compositions around Or_{90} regardless of grade or occurrence.

2.5.3 Chlorite

Few good chlorite analyses were obtained from rocks outside the aureole owing to the chlorite's fine grainsize and strong alteration. All chlorite analyses taken from such rocks showed interference effects related to the associated fine quartz and feldspar. Assuming that Mg/Fe+Mg ratios

would be little affected by this interference, it appears that no consistent changes in the Mg/Fe+Mg ratios of the chlorites occurred with the incoming of biotite. Similarly, the Al^{VI} content of the chlorites is often quoted to increase with the incoming of biotite (e.g. Pinsent and Smith, 1975; Katagas, 1980). However, analysed chlorites from outside the aureole, showing apparently only quartz interference (no extra alkali) gave very similar Al^{VI}/Fe+Mg ratios to those within the biotite zone.

Retrograde chlorite is present at temperatures above the cordierite isograd. It occurs with cordierite, and its Mg/Mg+Fe ratios are intermediate to those of biotite and cordierite for a given sample. Therefore, the retrograde formation of chlorite seems to involve the breakdown of cordierite + biotite.

2.5.4 Muscovite

From Table 2.2 the muscovites clearly become less phengitic on the higher-grade side of the biotite isograd. This has been recognised by several previous authors (e.g. Ernst, 1963; Mather, 1970; Katagas, 1980). Prograde and retrograde (after cordierite) muscovites (phengites) in sample M80, from the cordierite + K-feldspar zone, have identical compositions. Similarly, no compositional differences were obvious between the coarse muscovite plates and the finer aggregates (described in Section 2.4.4).

2.5.5 Biotite

Representative analyses of biotites are given in Tables 2.2 and 2.3. Variations in biotite chemistry with grade are illustrated in Figs. 2-3A→D. Based on Fig. 2-3A the composition of the biotite tetrahedral site appears to remain constant. Similarly, although more variable than Al^{IV}, Al^{VI} is relatively constant with increasing grade (Fig. 2-3B). The graph of Mg/Mg+Fe against distance from the contact (Fig. 2-3C) shows two sharp changes, which correlate with the two higher-grade zone boundaries. At approximately 500m from the contact, with the beginning of the cordierite + K-feldspar zone, the Mg/Mg+Fe ratio decreases sharply. Then, at approximately 100m from the contact biotite becomes richer in Mg, and has Mg contents similar to those in the cordierite zone. Within individual zones, biotite Mg/Mg+Fe ratios vary between samples, presumably reflecting variations in host-rock composition. Two curves are shown in Fig. 2-3D

TABLE 2.2. Representative microprobe analyses of minerals from lower-grade zones in the Walcha Road aureole

ZONE	OUTSIDE AUREOLE		BIOTITE ZONE						CORDIERITE ZONE				
SAMPLE NO.	M91	M91	26201	26201	26201	M11	26201	26201	M16	407	10A	11985	M16
MINERAL*	Phen	Phen	Chl	Chl	Phen	Phen	Bi	Bi	Phen	Phen	Bi	Bi	Cd
SiO_2	46.05	46.57	25.35	24.38	45.34	45.90	35.61	34.56	46.22	45.45	35.44	35.71	48.00
TiO_2	0.62	0.45	0.15	-	0.29	0.31	1.60	2.05	0.29	0.36	2.03	1.85	-
Al_2O_3	28.07	27.38	20.94	21.46	35.79	36.32	19.33	18.52	36.22	36.21	20.55	20.21	32.40
FeO**	4.26	3.78	26.34	26.88	0.71	0.83	20.70	20.74	0.93	0.88	20.14	20.03	8.75
MnO	-	-	0.44	0.53	-	-	0.14	-	-	-	-	0.22	0.81
MgO	2.38	2.53	14.07	13.66	0.38	0.34	8.51	8.18	0.46	0.38	8.14	7.91	7.08
CaO	-	-	-	-	-	-	0.11	0.18	-	-	-	-	-
Na_2O	0.22	0.17	0.29	0.37	0.39	0.36	0.16	0.17	0.72	0.48	0.25	0.33	0.41
K_2O	10.09	9.91	-	-	10.52	10.84	9.74	9.69	10.35	10.43	9.05	9.07	-
Total	91.69	90.79	87.58	87.28	93.42	94.90	95.90	94.09	95.19	94.19	95.60	95.33	97.45
Structural formulae†													
Si	6.476	6.582	5.393	5.237	6.133	6.122	5.425	5.391	6.137	6.101	5.367	5.427	5.016
Al^{IV}	1.524	1.418	2.607	2.763	1.868	1.879	2.575	2.609	1.863	1.899	2.633	2.574	0.984
Al^{VI}	3.133	3.147	2.648	2.674	3.842	3.835	0.899	0.799	3.810	3.834	1.038	1.049	3.010
Ti	0.066	0.048	0.024	-	0.030	0.031	0.183	0.241	0.029	0.036	0.231	0.211	-
Fe^{2+}	0.501	0.447	4.687	4.829	0.080	0.093	2.637	2.706	0.103	0.099	2.551	2.546	0.765
Mn	-	-	0.079	0.096	-	-	0.018	-	-	-	-	0.028	0.072
Mg	0.499	0.533	4.461	4.373	0.077	0.068	1.932	1.902	0.091	0.076	1.837	1.791	1.103
Ca	-	-	-	-	-	-	0.018	0.030	-	-	-	-	-
Na	0.06	0.047	0.120	0.154	0.102	0.093	0.047	0.051	0.185	0.125	0.073	0.097	0.083
K	1.810	1.787	-	-	1.815	1.844	1.893	1.929	1.753	1.786	1.749	1.758	-
Total Cations	14.069	14.008	20.019	20.126	13.946	13.964	15.628	15.657	13.971	13.956	15.480	15.481	11.032
Y GROUP	4.198	4.174	11.899	11.972	4.029	4.026	5.669	5.647	4.033	4.045	5.658	5.626	-
X GROUP	1.870	1.834	0.120	0.154	1.918	1.938	1.958	2.010	1.939	1.911	1.822	1.856	-
$Mg/Mg+Fe^{2+}$	0.499	0.544	0.488	0.475	0.488	0.422	0.423	0.413	0.468	0.435	0.419	0.413	0.590

†Biotite and phengite based on 22 oxygens
Chlorite based on 28 oxygens
Cordierite based on 18 oxygens

**Total Fe as FeO

* Bi = biotite, Phen = phengite, Chl = chlorite, Cd = cordierite

Figure 2-3: Biotite chemistry versus distance from the contact of the Walcha Road Adamellite.

Symbols: ● southeast contact aureole

× southwest contact aureole

■ western contact aureole

▲ sample 64 (see text)

open symbols refer to samples of migmatite.

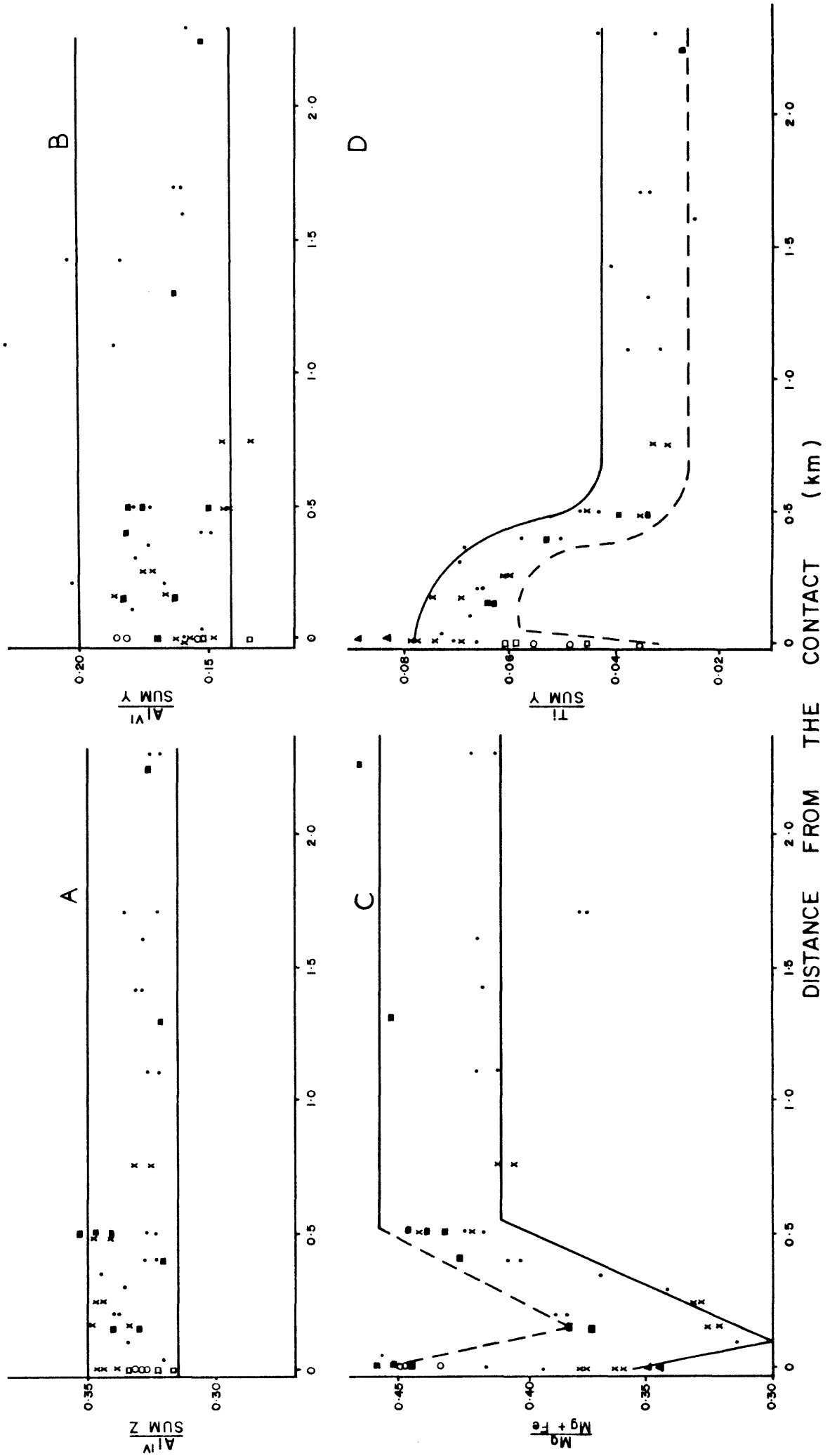
A
B
C
D
$\frac{Al^{IV}}{SUM\ Z}$
$\frac{Al^{VI}}{SUM\ Y}$
$\frac{Mg}{Mg + Fe}$
$\frac{Ti}{SUM\ Y}$
DISTANCE FROM THE CONTACT (km)

representing the extremes of this variation. The three localities are represented differently on this Figure, and less variation is seen between samples from the same locality.

Fig. 2-3D shows a marked increase in Ti content of the biotites with the incoming of cordierite + K-feldspar. This increase "levels off" in the cordierite + K-feldspar ± garnet zone, and although the biotite compositions in the migmatitic rocks are variable, they appear to show a decrease in the Ti content at the contact in the eastern and western localities.

This trend in Ti with increasing temperature is broadly opposite that of the Mg/Mg+Fe ratio (Fig. 2-3C). As the Al^{VI} content in the biotites is relatively constant, this inverse relationship between biotite Ti content and Mg/Mg+Fe ratio is in agreement with Guidotti *et al.* (1977) and Gorbatschev (1968,1977). This relationship also holds between samples of equivalent grade (the more Mg-rich samples, notably those from the western locality, are generally poorer in Ti), and between grains in individual samples (e.g. sample 391, Tables 2.3 and 2.6).

Since a large proportion of Ti in the pelites occurs within the biotites, a modal decrease in biotite with increasing grade, as in the cordierite + K-feldspar and cordierite + K-feldspar ± garnet zones (Section 2.4), would be expected to increase the biotite Ti content. However, this is modified by the above relationship between biotite Ti content and Mg/Mg+Fe ratio. Therefore, in the cordierite + K-feldspar zone, with a decrease in the Mg/Mg+Fe ratio of biotite, Ti content of the biotite increases sharply. However, in the cordierite + K-feldspar ± garnet zone, where the Mg/Mg+Fe ratio of the biotite tends to increase, the trend for increasing Ti is "levelled off" (and possibly reversed). In very Fe-rich rocks, though, high biotite Ti contents are found at the contact (e.g. sample 64, Fig. 2-3D).

The biotites show an increase in their Al^{VI}/Fe+Mg ratio from an average of around 0.19 to around 0.25 across the cordierite isograd. At this boundary, a slight decrease in the biotite Na/Na+K ratio is also recorded from 0.03 → 0.05. Both these changes agree with those reported by Ramsay (1974) for the same boundary in metasediments of the Slave

TABLE 2.3. Representative microprobe analyses of minerals from higher-grade zones in the Walcha Road aureole

	CORDIERITE + K-FELDSPAR ZONE → INCREASING GRADE								CORDIERITE + K-FELDSPAR ± GARNET ZONE							
SAMPLE NO.	M80	M80	26212	26212	M78	M78	26213	26213	64	64	64	391	391	391	349	349
MINERAL	Bi	Cd	Bi	Cd	Bi	Cd	Bi	Cd	Bi	Cd	Gt	Bi	Cd	Gt	Bi	Gt
SiO_2	33.57	48.89	34.15	48.33	33.47	47.51	34.69	48.63	35.29	48.12	36.78	34.88	48.58	37.81	37.49	36.81
TiO_2	2.08	-	3.28	0.10	2.90	-	3.23	-	4.25	-	-	1.74	-	-	0.72	-
Al_2O_3	19.22	30.32	20.57	32.83	20.45	32.33	20.25	33.14	18.13	33.25	21.49	20.21	32.66	21.60	19.76	20.98
FeO**	20.46	7.95	20.53	9.87	21.97	11.44	22.15	11.39	22.05	11.17	32.72[x]	18.70	9.12	30.76	22.68	37.96
MnO	0.25	0.87	0.17	0.58	-	0.28	-	-	0.24	0.88	5.38	0.29	0.52	6.78	-	3.94
MgO	8.37	6.61	6.78	6.74	6.10	6.47	5.69	6.32	6.64	6.21	2.42	8.63	7.28	3.31	2.48	0.40
CaO	0.10	-	0.09	-	0.11	-	-	-	-	0.12	0.16	-	-	0.78	0.16	0.46
Na_2O	0.15	1.36	0.17	0.17	-	0.34	0.17	0.23	0.58	0.42	-	-	0.39	-	0.27	-
K_2O	9.18	-	9.77	-	9.34	-	9.65	-	8.96	-	-	9.78	-	-	8.51	-
Total	93.38	96.00	95.51	98.62	94.34	98.37	95.83	99.71	96.14	100.17	100.01	94.23	98.55	101.05	92.07	100.56
Structural formulae[†]																
Si	5.269	5.178	5.235	5.005	5.222	4.973	5.323	5.001	5.397	4.952	5.949	5.362	5.019	6.007	5.911	6.014
Al^{IV}	2.731	0.822	2.765	0.995	2.778	1.027	2.677	0.999	2.603	1.048	0.051	2.638	0.981	-	2.089	-
Al^{VI}	0.828	2.967	0.954	3.015	0.985	2.964	0.988	3.021	0.668	2.988	4.045	1.027	2.100	4.045	1.586	4.040
Ti	0.246	-	0.378	0.008	0.340	-	0.373	-	0.489	-	-	0.201	-	-	0.085	-
Fe^{2+}	2.686	0.704	2.632	0.855	2.867	1.001	2.843	0.980	2.820	0.961	4.427	2.404	0.788	4.088	2.991	5.187
Mn	0.033	0.078	0.022	0.051	-	0.025	-	-	0.031	0.077	0.737	0.038	0.046	0.912	-	0.545
Mg	1.958	1.043	1.549	1.040	1.418	1.009	1.301	0.969	1.513	0.952	0.584	1.977	1.121	0.784	0.583	0.097
Ca	0.017	-	0.015	-	0.018	-	-	-	-	0.013	0.201	-	-	0.133	0.027	0.081
Na	0.046	0.279	0.051	0.034	-	0.069	0.051	0.046	0.172	0.084	-	-	0.078	-	0.083	-
K	1.838	-	1.911	-	1.859	-	1.889	-	1.748	-	-	1.918	-	-	1.712	-
Total cations	15.652	11.070	15.511	11.003	15.488	11.069	15.444	11.015	15.441	11.075	15.949	15.566	11.033	15.969	15.066	15.974
Y - GROUP	5.750		5.535		5.611		5.505		5.521			5.647			5.245	
X - GROUP	1.901		1.976		1.878		1.940		1.920			1.918			1.821	
$Mg/Mg+Fe^{2+}$	0.422	0.597	0.370	0.549	0.331	0.502	0.314	0.497	0.349	0.498	0.116	0.451	0.587	0.161	0.163	0.018
											Al 74.42 Sp 12.39 Py 9.81 An 0.16 Gr 3.22			Al 69.08 Sp 15.42 Py 13.25 An 0.03 Gr 2.21		Al 87.76 Sp 9.23 Py 1.65 An 0.03 Gr 1.33

† biotite based on 22 oxygens; cordierite based on 18 oxygens; garnet based on 24 oxygens
x also contains 0.05 Fe_2O_3 as calculated by Hamm and Vieten (1971)
** total Fe as FeO
Abbreviations: Bi = biotite, Cd = cordierite, Gt = garnet, Al = almandine, Sp = spessartine, Py = pyrope, An = andradite, Gr = grossular.

Craton of northern Canada.

2.5.6 Cordierite

Representative analyses are given in Tables 2.2 and 2.3, and the graph of Mg/Fe+Mg against distance is shown in Fig. 2-4. From Fig. 2-4 a marked decrease in the Mg/Mg+Fe ratio of cordierite is noted at the beginning of the cordierite + K-feldspar zone. But within the cordierite + K-feldspar ± garnet zone the Mg content increases back to higher values. These changes are identical to those recognised in biotite.

Cordierite analyses are not as numerous as those of biotite because the cordierite is typically retrogressed. As noted in Section 2.4.3, a common alteration product of the cordierite is a yellow isotropic material. Many attempted cordierite analyses proved to be a mixture of the original cordierite and this material. As the cordierite alters, its original Mg/Mg+Fe ratio progressively decreases, Fe, Mn and Mg decrease, and Ca, Na and K generally increase. If such changes in mineral chemistry are allowed for, rough estimates of the original cordierite Mg/Mg+Fe ratio can be made. Three such estimates of mildly altered grains are shown in Fig. 2-4, and agree broadly (though possibly having slightly high Mg/Mg+Fe values) with the trends based on fresh cordierite analyses. Analyses of the alteration material and its partial alteration of fresh cordierite are shown in Table 2.4.

2.5.7 Garnets

Analyses of garnets associated with cordierite and biotite are given in Table 2.3. These are almandine-rich garnets, but with a significant spessartine component. One sample (349, described in Section 2.4.5) contains exceptionally Fe-rich garnets (88% almandine) associated with very Fe-rich biotites. This reflects the low Mg/Mg+Fe ratio of the host rock. The influence of temperature on garnet composition cannot be reliably ascertained because of the restricted width (i.e. temperature range) of the cordierite + K-feldspar ± garnet zone, and the limited number of garnet-bearing samples.

2.5.8 Opaques

Both hematite and ilmenite occur within the pelites outside the

Figure 2-4: Cordierite Mg/Mg+Fe ratio (χ^{Cd}_{Mg}) versus distance from the contact of the Walcha Road Adamellite.

Symbols:

- ● southeast contact aureole
- ✕ southwest contact aureole
- ■ western contact aureole
- ▲ sample 64 (see text)
- ⬯ analyses corrected for alteration - southeast contact aureole
- o migmatite sample (391) - southeast contact aureole

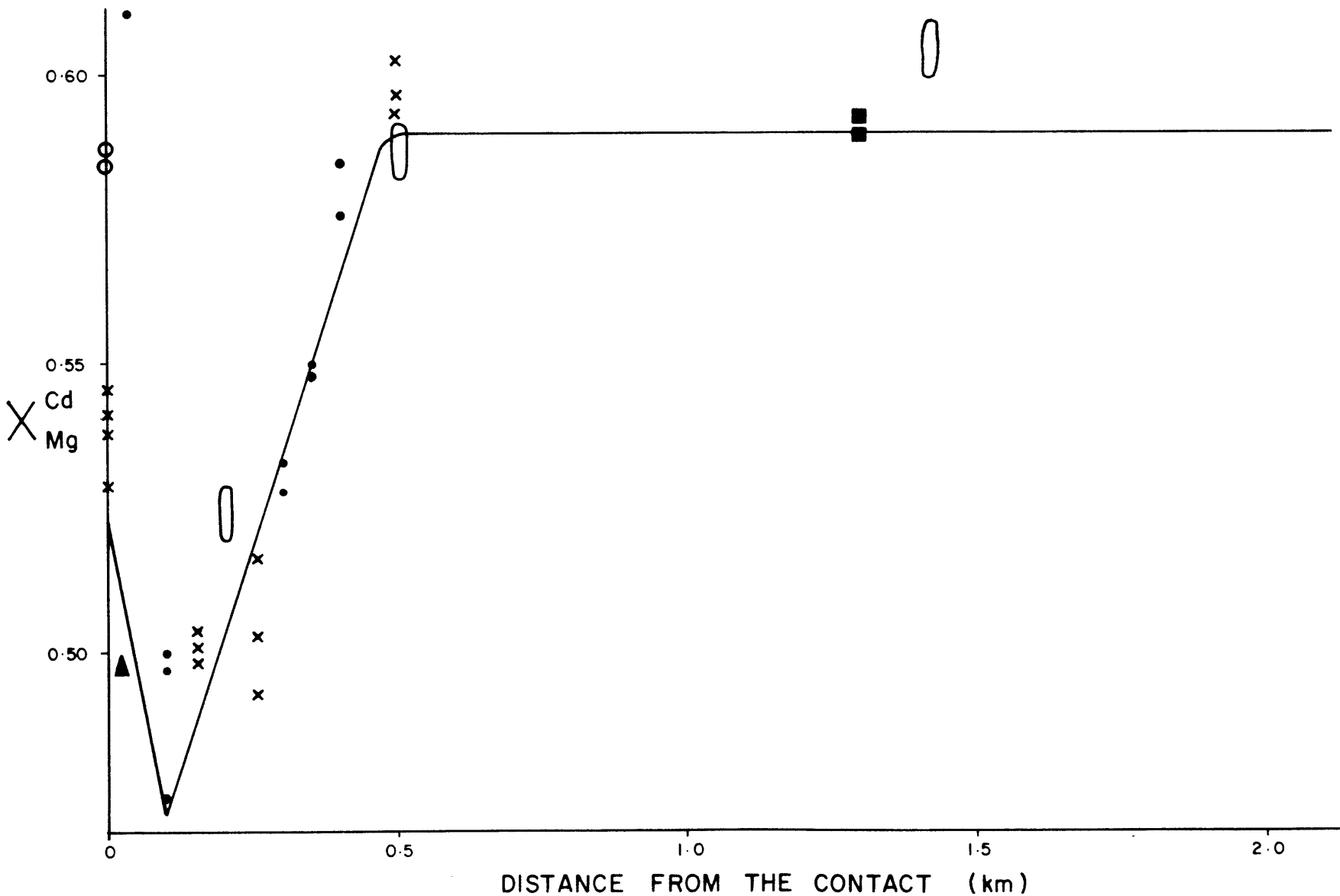
0·60
0·55
0·50
Cd
Mg
0
0·5
1·0
1·5
2·0
DISTANCE FROM THE CONTACT (km)

TABLE 2.4. Microprobe analyses showing the effects of progressive cordierite alteration

Sample No.	26213 FRESH	26213 ALTERED	26213 VERY ALTERED	11981 FRESH	11981 SLIGHTLY ALTERED	11981 ALTERED	407 TOTALLY	M10 ALTERED
SiO_2	48.63	42.87	43.41	48.70	44.31	44.13	48.66	42.60
TiO_2	-	-	-	-	-	0.20	-	0.10
Al_2O_3	33.14	30.14	35.98	33.02	31.29	30.80	32.41	28.55
FeO†	11.39	8.43	4.01	10.19	8.76	6.70	0.40	0.37
MnO	-	-	-	0.94	0.65	.24	-	-
MgO	6.32	3.62	1.66	6.50	4.52	2.59	0.15	0.19
CaO	-	0.42	-	-	0.14	1.29	0.39	0.52
Na_2O	0.23	0.11	0.10	-	-	0.27	0.16	0.10
K_2O	-	0.91	0.12	-	-	0.88	0.16	0.29
TOTAL	99.71	86.50	85.28	99.35	89.67	87.10	82.33	72.72
Si	5.001	5.056	4.995	5.015	5.025	5.128	5.619	5.586
Al^{IV}	0.999	0.944	1.006	0.985	0.975	0.872	0.381	0.414
Al^{VI}	3.021	3.249	3.877	3.026	3.211	3.350	4.291	4.002
Ti	-	-	-	-	-	0.018	-	0.010
Fe^{2+}	0.980	0.832	0.386	0.878	0.831	0.651	0.039	0.041
Mn	-	-	-	0.082	0.062	0.024	-	-
Mg	0.969	0.636	0.285	0.998	0.764	0.449	0.026	0.037
Ca	-	.053	-	-	0.017	0.161	0.048	0.073
Na	0.046	0.025	0.022	-	-	0.061	0.036	0.026
K	-	0.137	0.018	-	-	0.131	0.024	0.049
TOTAL CATIONS	11.015	10.932	10.588	10.983	10.885	10.842	10.464	10.239
Mg/Mg+Fe	0.497	0.433	0.425	0.532	0.479	0.408	0.400	0.474

All structural formulae based on 18 oxygens

† Total Fe as FeO

TABLE 2.5. Microprobe ilmenite analyses from pelites of varying grade in the Walcha Road aureole

ZONE		BIOTITE ZONE			CORDIERITE ZONE			CORD + K-F ZONE			
SAMPLE NO.	26215†	26201	M20	26198	11985	M82	M11	M78	M76	26213	64x
DISTANCE*	4500m	2300m	2250m	1700m	1100m	750m	500m	250m	160m	100m	10m
SiO_2	0.44	0.55	0.41	0.50	0.37	0.47	0.34	0.96	0.21	0.45	0.23
TiO_2	46.43	52.83	54.35	52.62	52.79	1.995	52.65	52.19	51.54	53.16	53.46
Al_2O_3	1.20	-	0.21	0.45	-	-	0.12	0.39	-	0.11	0.27
FeO**	36.62	41.41	37.69	42.35	43.34	41.83	29.00	43.25	44.32	46.03	32.67
MnO	3.60	3.92	7.79	3.26	3.64	4.12	17.34	0.84	0.78	0.65	12.44
MgO	0.28	-	-	-	0.11	-	-	-	0.10	0.16	0.21
CaO	0.62	0.10	-	-	0.20	0.11	-	0.19	-	-	-
Na_2O	1.09	-	-	-	-	-	-	0.27	-	0.15	0.31
K_2O	-	0.16	-	0.07	-	-	0.09	0.16	0.11	-	-
Total	90.28	98.97	100.45	99.25	100.45	98.67	99.55	98.25	97.06	100.71	99.59
Structural formulae based on six oxygens											
Si	0.024	0.028	0.020	0.025	0.019	0.024	0.017	0.049	0.011	0.022	0.012
Al	0.078	-	0.123	0.027	-	-	0.007	0.023	-	0.007	0.016
Ti	1.928	2.008	2.026	1.993	1.988	1.995	1.995	1.986	2.007	1.991	2.013
Fe^{2+}	1.691	1.750	1.562	1.783	1.815	1.780	1.222	1.831	1.919	1.917	1.368
Mn	0.168	0.168	0.327	0.139	0.154	0.178	0.740	0.036	0.034	0.027	0.528
Mg	0.023	-	-	-	0.008	-	-	-	0.008	0.012	0.016
Ca	0.037	0.005	-	-	0.011	0.006	-	0.010	-	-	-
Na	0.117	-	-	-	-	-	-	0.027	-	0.015	0.030
K	-	0.010	-	0.005	-	-	0.006	0.010	0.007	-	-
Total Cations	4.066	3.969	4.058	3.972	3.995	3.983	3.987	3.972	3.986	3.991	3.983
Mg/Mn+Fe	0.090	0.086	0.173	0.072	0.078	0.091	0.377	0.019	0.017	0.014	0.278

* Distance from the igneous contact

x Garnet-bearing sample from the southern contact of Mt Duval Adamellite (see text)

† A sample from outside the Walcha Road aureole

** Total Fe as FeO

aureole. However, in the contact-metamorphosed rocks, ilmenite is the prominent opaque phase. Ilmenite analyses are shown in Table 2.5. The ilmenites are moderately uniform in composition at the lower grades, although a few Mn-rich ilmenites do occur (e.g. M11), but in the cordierite + K-feldspar zone they show a marked decrease in their Mn/Mn+Fe ratios from around 0.090 to 0.017. Ilmenite within the garnet-containing rock (64) is Mn-rich (Mn/Mn+Fe = 0.278). This probably reflects the high Mn content of the host rock, which may be a possible requirement for garnet formation in these pelitic rocks (discussed further in Section 2.7).

2.6 METAMORPHIC REACTIONS

2.6.1 Introduction

This section discusses the changes in pelitic mineralogy with increasing grade (shown on AKF and AFM diagrams, Figs. 2-5A→E and Figs. 2-6A→E respectively), and proposes balanced reaction equations, based on microprobe analyses, to represent these changes. Whole-rock compositions, from Table 2.1, are plotted on the AKF diagrams. However, as discussed in Section 2.2, these analyses are mixtures of pelitic and quartzo-feldspathic layers and therefore they will only broadly represent the host-rock compositions of the pelitic assemblages. Major differences between the whole-rock compositions of Table 2.1 and actual host-rock compositions of the pelitic assemblages would be caused by the presence of K-feldspar in the quartzo-feldspathic layers. This would result in plots in the AKF diagram that are too close to the K corner to accurately represent the pelitic assemblages, which could apply to the analyses of samples 391 and 64. Section 2.7 discusses the discontinuous or continuous characteristics of the observed reactions in terms of their associated phase relations.

2.6.2 Biotite Isograd

The reaction for biotite formation has been widely discussed in the literature on psammitic and pelitic rocks (e.g. Ernst, 1963; Mather, 1970; Brown, 1971,1975; Ramsay, 1973; Pinsent and Smith, 1975; Katagas, 1980). Outside the Walcha Road aureole, K-feldspar + muscovite (phengite) + chlorite is stable (Fig. 2-5A), but with the incoming of biotite the

Figure 2-5: AKF diagrams for the Walcha Road Adamellite contact aureole

Symbols: $A = Al_2O_3 + Fe_2O_3 - (Na_2O + K_2O + CaO)$

$K = K_2O$

$F = FeO + MnO + MgO$

All oxides expressed in molecular proportions.
Mineral compositions are based on probe analyses.
All assemblages contain quartz and plagioclase.
Both hematite and ilmenite occur outside the aureole. However, ilmenite predominates within the metamorphic zones.
Muscovite shown in Fig. 2-5D refers to muscovite stable in the outer part of the cordierite + K-feldspar zone.
Whole-rock compositions (Table 2.1) are plotted as crosses, and labelled in Fig. 2-5A.

A) OUTSIDE THE AUREOLE

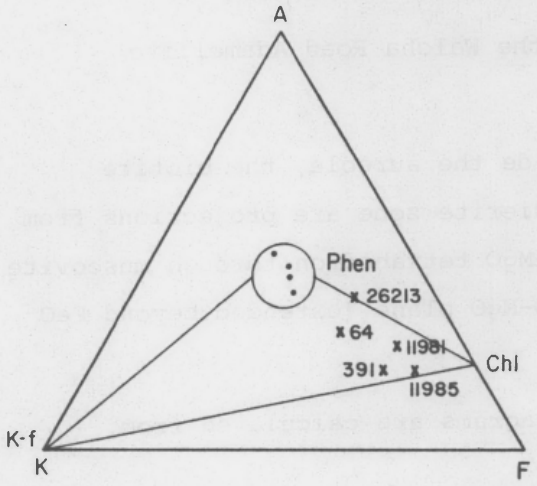

T

B) BIOTITE ZONE

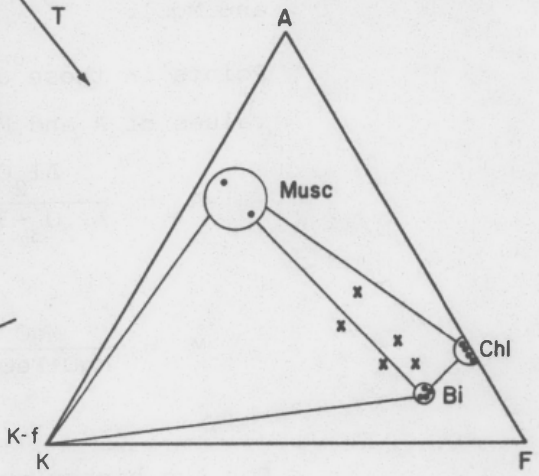

C) CORDIERITE ZONE

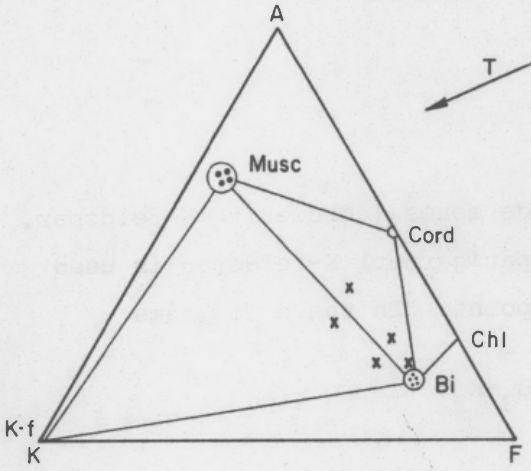

T

D) CORD. + K-F. ZONE

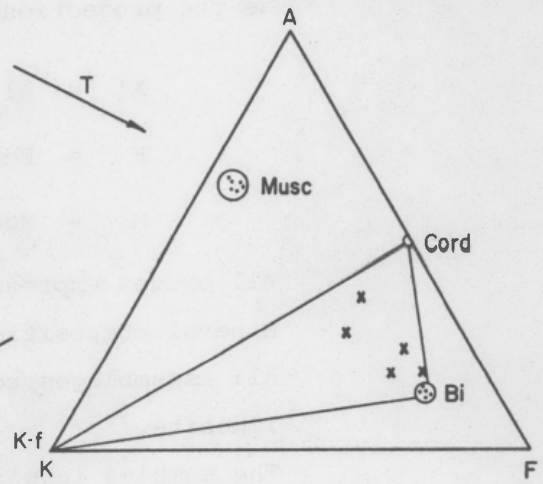

T

E) CORD. + K-F. ± GT. ZONE

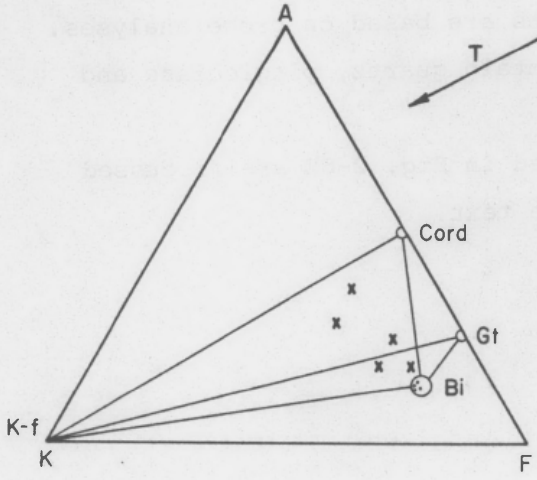

T

Figure 2-6: AFM diagrams for the Walcha Road Adamellite contact aureole.

Diagrams for outside the aureole, the biotite zone, and the cordierite zone are projections from the K_2O-Al_2O_3-FeO-MgO tetrahedron through muscovite onto the Al_2O_3-FeO-MgO plane (extended beyond FeO and MgO).

Points in these diagrams are calculated from values of A and M:

$$A = \frac{Al_2O_3 - 3K_2O}{Al_2O_3 - 3K_2O + MgO + FeO}$$

$$M = \frac{MgO}{MgO + FeO}$$

For the higher-grade zones (cordierite+K-feldspar, cordierite+K-feldspar±garnet) K-feldspar is used as the projection point. In these diagrams

$$A' = Al_2O_3 - K_2O$$

$$F = FeO$$

$$M = MgO$$

All oxides expressed in molecular proportions.
Mineral compositions are based on probe analyses.
All assemblages contain quartz, plagioclase and ilmenite.
The samples labelled in Fig. 2-6E are discussed individually in the text.

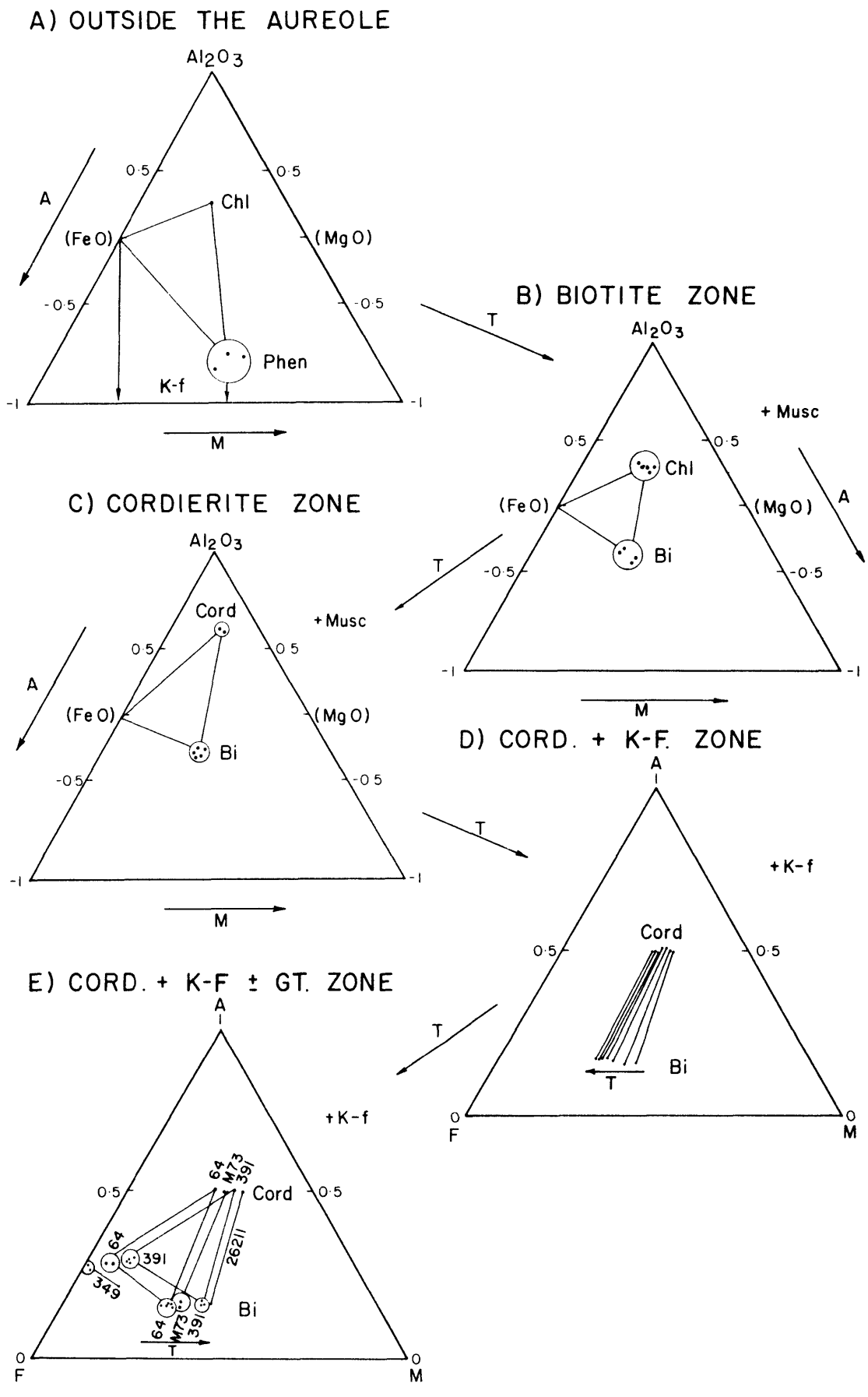
A) OUTSIDE THE AUREOLE
Al2O3
0·5
0·5
A
Chl
(Fe O)
(Mg O)
-0·5
-0·5
Phen
K-f
-1
-1
M
B) BIOTITE ZONE
T
Al2O3
+ Musc
0·5
0·5
Chl
(Fe O)
(Mg O)
A
Bi
T
-0·5
-0·5
-1
-1
M
C) CORDIERITE ZONE
Al2O3
Cord
+Musc
0·5
0·5
A
(Fe O)
(Mg O)
Bi
-0·5
-0·5
-1
-1
M
D) CORD. + K-F. ZONE
A
T
+K-f
Cord
0·5
0·5
T
Bi
0
F
0
M
E) CORD. + K-F ± GT. ZONE
A
+K-f
64
M73
391
0·5
Cord
0·5
64
391
26211
349
Bi
64
M73
391
T
0
F
0
M

K-feldspar-chlorite tie-line is broken (Fig. 2-5B). The biotite composition falls on the low-Al side of the K-feldspar-muscovite-chlorite field defined by the pelites outside the aureole (compare Figs. 2-5A and 2-5B). Therefore, as documented by Mather (1970), the formation of biotite from the earlier pelitic assemblage is associated with the appearance of less-phengitic muscovite (noted in Section 2.5.4). Fe oxides are stable both outside the aureole and in the biotite zone (Figs. 2-6A and B respectively).

The iron oxides are likely to be involved in the biotite-forming reaction, because the biotite has lower Mg/Mg+Fe ratios than either the chlorite or phengite occurring outside the aureole, and neither of the latter minerals shows any significant increase in magnesium with the incoming of biotite (Section 2.5). The Ti content in the biotite suggests that at least some of the required Fe oxide is ilmenite. The proposed equation for this reaction based on probe data is:

1.0 Chlorite + 3.0 Muscovite(1) + 4.4 K-feldspar + 0.25 Ilmenite + 0.59 Hematite

$\rightarrow$ 3.0 Biotite + 2.2 Muscovite(2) + 8.67 Quartz + 3.6 H_2O (2-I)

Reactants

Chlorite	$Fe_{4.70}Mn_{.05}Mg_{4.40}Al_{2.75}Si_{5.4}Al_{2.6}O_{20}(OH)_{16}$
Muscovite(1)	$K_{1.80}Na_{.05}Al_{3.05}Ti_{.04}Fe_{.55}Mg_{.55}Si_{6.6}Al_{1.4}O_{20}(OH)_4$
K-feldspar	$K_{.90}Na_{.10}Al_1Si_3O_8$
Ilmenite	$Fe_{1.83}Mn_{.17}Ti_2O_6$

Products

Biotite	$K_{1.80}Na_{.10}Al_{.95}Ti_{.18}Fe_{2.60}Mn_{.03}Mg_{1.95}Si_{5.4}Al_{2.6}O_{20}(OH)_4$
Muscovite(2)	$K_{1.80}Na_{.12}Al_{3.82}Ti_{.04}Fe_{.09}Mg_{.08}Si_{6.15}Al_{1.85}O_{20}(OH)_4$.

The presence of K-feldspar in pelites outside the aureole has been verified by probe analysis. However, K-feldspar is rare in the biotite zone and appears to be consumed by reaction 2-I. Hematite also appears to be lost across this reaction boundary, but all other minerals present outside the aureole persist into the biotite zone.

Other work on the incoming of biotite has shown no K-feldspar in the sediments on the lower-grade side of the biotite boundary (e.g. Ernst, 1963; Ramsay, 1973; Pinsent and Smith, 1975; Katagas, 1980). Such rocks, as discussed by Mather (1970), are richer in Al (more pelitic)

than those containing K-feldspar, and plot outside the phengite-chlorite-K-feldspar triangle. In pelites initially lacking K-feldspar, the above authors suggest that biotite could form mainly by the breakdown of chlorite and muscovite with the formation of less-phengitic muscovite (e.g. Chlorite + Muscovite(1) → Biotite + Muscovite(2) + Quartz + H_2O, Ernst, 1963). Chlorite may also become richer in Al as suggested by Pinsent and Smith (1975), Winkler (1976) and Katagas (1980). Mather (1970) has noted that biotite will appear at higher temperatures in these more Al-rich rocks. However, as the pelites outside the Walcha Road aureole typically contain K-feldspar, the effect of this has not been seen, and the incoming of biotite is quite abrupt. It is feasible, though, that as K-feldspar is exhausted by reaction 2-I, some further biotite may form via the muscovite + chlorite breakdown reaction. Based on the mineral compositions used in reaction 2-I a possible balanced equation is

1.0 Chlorite + 15.0 Muscovite(1) + 0.43 Ilmenite + 1.50 Hematite → 6.13 Biotite + 8.87 Muscovite(2) + 16.75 Quartz + 8 Water.

2.6.3 Cordierite Isograd

The beginning of the cordierite zone is sharply defined in the field, and is represented on the AKF diagram (Fig. 2-5C) by the appearance of the cordierite-biotite tie-line at the expense of the tie-line between chlorite and muscovite (i.e. muscovite + chlorite + quartz → cordierite + biotite + water). The new assemblage contains biotite, cordierite, muscovite, and minor ilmenite, with chlorite typically consumed at this boundary (Figs. 2-5C and 2-6C).

A reaction of this form to account for the low-grade formation of cordierite has been investigated by several authors, both petrologically (e.g. Schreyer and Yoder, 1961; Ramsay, 1974) and experimentally (e.g. Hess, 1969; Seifert, 1970; Bird and Fawcett, 1971). In particular Ramsay (1974), though dealing with slightly more magnesian rocks, has presented a cordierite-forming reaction which is very similar to that derived from the data of this study. In this study, biotite increases in amount (Section 2.4.3) and in its Na/Na+K and Al/Fe+Mg ratios across the cordierite isograd, without any change in its Mg/Mg+Fe ratio (Section 2.5.5). These compositional changes were also observed by Ramsay (1974) who, though, also noted a change in the $Si/Si+Al^{IV}$ ratio of the biotites,

which was not found in this study. Muscovite loses most of its phengitic character across the biotite boundary, and no further change in its composition was noted in the Walcha Road aureole with the incoming of cordierite. The suggested equation based on probe data is

1.0 Chlorite + 1.33 Muscovite + 1.0 Biotite(1) + 0.14 Ilmenite + 3.95 Quartz

→ 2.05 Cordierite + 2.33 Biotite(2) + 8 Water (2-II)

Reactants

Chlorite $Fe_{4.70}Mn_{.07}Mg_{4.40}Al_{2.75}Si_{5.3}Al_{2.7}O_{20}(OH)_{16}$

Muscovite $K_{1.80}Na_{.10}Al_{3.82}Ti_{.04}Fe_{.09}Mg_{.08}Si_{6.15}Al_{1.85}O_{20}(OH)_4$

Biotite(1) $K_{1.80}Na_{.10}Al_{.95}Ti_{.18}Fe_{2.60}Mn_{.02}Mg_{1.95}Si_{5.4}Al_{2.6}O_{20}(OH)_4$

Ilmenite $Fe_{1.80}Mn_{.20}Ti_2O_6$

Products

Cordierite $Al_{3.00}Fe_{.80}Mn_{.05}Mg_{1.10}Si_5AlO_{18}$

Biotite(2) $K_{1.80}Na_{.10}Al_{1.00}Ti_{.22}Fe_{2.55}Mn_{.01}Mg_{1.80}Si_{5.4}Al_{2.6}O_{20}(OH)_4$

Previous authors have commonly noted the simultaneous appearance of cordierite and an Al-silicate (e.g. Hess, 1969; Guidotti *et al.*, 1975; Winkler, 1976). This does not occur in the Walcha Road aureole, nor in the rocks studied by Ramsay (1974). The absence of an Al-silicate may be dependent on pressure, as Seifert (1970) found that at higher pressures the cordierite-muscovite tie-line is replaced by biotite-Al-silicate. However, Winkler (1976) has presented data on the reaction:

Chlorite + Muscovite + Quartz → Cordierite + Biotite + Al-silicate + H_2O

at very low pressures. The absence of Al-silicate therefore appears to be a compositional feature (further discussed in Section 2.7.3).

2.6.4 Cordierite + K-feldspar Isograd

The reaction responsible for the incoming of cordierite + K-feldspar is broadly that described by Seifert (1976), Winkler (1976) and Hoffer (1978) involving the breakdown of muscovite + biotite (i.e. Muscovite + Biotite + Quartz → Cordierite + K-feldspar + H_2O). Muscovite is consumed by this reaction producing a cordierite + biotite + K-feldspar assemblage. This is shown on the AKF diagram (Fig. 3-5D), and reflects the whole-rock compositions lying to the biotite side of the cordierite-K-feldspar tie-line. This is not a sharp boundary as prograde muscovite

and biotite have been found with quartz + cordierite + K-feldspar past the cordierite + K-feldspar isograd (Section 2.4.4). A general increase in cordierite and K-feldspar and a decrease in biotite have been noticed through the zone with increasing grade. Therefore, the reaction appears to have occurred over a temperature interval. This is substantiated by the chemistry of the cordierite and biotite, which is shown in the AFM diagram (Fig. 2-6D) to continuously change toward lower values of Mg/Mg+Fe with increasing temperature. Because biotite, cordierite and ilmenite change composition across this zone boundary, these phases must be shown on both sides of the equation representing this boundary. Because the cordierite and biotite are continuously changing composition across the cordierite + K-feldspar zone (Section 2.5), no unique compositions exist for these products. Therefore, actual analyses typifying the change have been chosen to allow the reaction to be represented. The equation is given as

$$0.87\ \text{Muscovite} + 1.00\ \text{Biotite(1)} + 0.10\ \text{Cordierite(1)} + 0.28\ \text{Ilmenite(1)} + 4.54\ \text{Quartz} \rightarrow 2.31\ \text{K-feldspar} + 1.07\ \text{Cordierite(2)} + 0.65\ \text{Biotite(2)} + 0.28\ \text{Ilmenite(2)} + 2.44\ H_2O \qquad (2\text{-III})$$

Reactants

Muscovite	$K_{1.80}Na_{.10}Al_{3.82}Ti_{.03}Mg_{.08}Fe_{.09}Si_{6.15}Al_{1.85}O_{20}(OH)_4$
Biotite(1)	$K_{1.80}Na_{.10}Al_{1.00}Ti_{.22}Mg_{1.80}Mn_{.02}Fe_{2.55}Si_{5.40}Al_{2.60}O_{20}(OH)_4$
Cordierite(1)	$Al_{3.00}Fe_{.80}Mn_{.05}Mg_{1.10}Si_5Al_1O_{18}$
Ilmenite(1)	$Fe_{1.82}Mn_{.18}Ti_2O_6$

Products

K-feldspar	$K_{0.95}Na_{.05}AlSi_3O_8$
Cordierite(2)	$Al_{3.00}Fe_{.87}Mn_{.05}Mg_{.99}Si_5AlO_{18}$
Biotite(2)	$K_{1.80}Na_{.10}Al_{1.00}Ti_{.38}Fe_{2.67}Mn_{.02}Mg_{1.41}Si_{5.40}Al_{2.60}O_{20}(OH)_4$
Ilmenite(2)	$Fe_{1.97}Mn_{.03}Ti_2O_6$

The actual extent of the reaction (i.e. the degree of Mg/Mg+Fe change in the minerals) will be constrained by consumption of one of the reactants (e.g. muscovite), the whole-rock composition, or its intersection with another reaction (discussed in Section 2.7).

2.6.5 Garnet Isograd

As noted by Hoffer (1978), cordierite + K-feldspar assemblages need

not break down until temperatures sufficient for melting are reached. However, at the highest grades within the Walcha Road aureole garnet is able to form in pelites of appropriate composition. Mineral assemblages containing garnet lack muscovite and Al-silicate. Associated with the incoming of garnet is a further increase in K-feldspar, whereas both biotite and cordierite appear to decrease (Fig. 2-2, Section 2.4). The reaction is therefore believed to be

$$\text{Biotite} + \text{Cordierite} + \text{Quartz} \rightarrow \text{Garnet} + \text{K-feldspar} + H_2O$$

This reaction has not been investigated by many other authors as sillimanite is typically recorded in the lower-grade assemblage, and reactions such as

$$\text{Biotite} + \text{Sillimanite} + \text{Quartz} \rightarrow \text{Garnet} + \text{K-feldspar}$$

(e.g. Schmid and Wood, 1976) and

$$\text{Biotite} + \text{Sillimanite} + \text{Quartz} \rightarrow \text{Garnet} + \text{Cordierite} + \text{K-feldspar} + H_2O$$

(e.g. Holdaway and Lee, 1977) are usually suggested for the formation of garnet + K-feldspar. However, the formation of garnet + K-feldspar from biotite + cordierite + quartz is shown by Thompson (1976b) to be important at low-pressure, high-temperature conditions.

No phase, in the rocks examined, was totally consumed with the incoming of garnet. This is represented on the AKF diagram (Fig. 2-5E) by the appearance of the garnet-K-feldspar tie-line, with the cordierite-biotite tie-line retained. In Section 2.5 it was noted that biotite and cordierite associated with garnet have higher Mg/Mg+Fe ratios than in the cordierite + K-feldspar zone. Also, in garnet-containing rocks ilmenite is relatively Mn rich, and plagioclase is characteristically Na rich. The latter is associated with garnet containing a minor Ca component. Using probe analyses, equation 2-IV is given to represent the formation of garnet:

$$\begin{aligned}1.50\ \text{Biotite(1)} + 1.00\ \text{Cordierite(1)} + 1.00\ \text{Ilmenite(1)} + 1.89\ \text{Quartz} + \\ 0.66\ \text{Plagioclase(1)} + 0.98\ \text{MnO}\end{aligned}$$

$$\begin{aligned}\rightarrow 0.52\ \text{Garnet} + 0.95\ \text{K-feldspar} + 1.00\ \text{Biotite(2)} + 0.71\ \text{Cordierite(2)} + \\ 1.13\ \text{Ilmenite(2)} + 0.66\ \text{Plagioclase(2)} + 1.00\ H_2O\end{aligned} \qquad \text{(2-IV)}$$

Reactants

Biotite(1) $K_{1.80}Na_{.10}N_{1.00}Ti_{.38}Fe_{2.67}Mn_{.02}Mg_{1.41}Si_{5.4}Al_{2.6}O_{20}(OH)_4$

Cordierite(1) $Al_{3.00}Fe_{.87}Mn_{.05}Mg_{.99}Si_5AlO_{18}$

Ilmenite(1)	$Fe_{1.97}Mn_{.03}Ti_2O_6$
Plagioclase(1)	$Na_{.67}Ca_{.33}Al_{1.33}Si_{2.67}O_8$
Products	
Garnet	$Al_{4.00}Fe_{4.04}Mn_{1.07}Mg_{.70}Ca_{.14}Si_6O_{24}$
K-feldspar	$K_{.95}Na_{.05}AlSi_3O_8$
Biotite(2)	$K_{1.80}Na_{.10}Al_{1.00}Ti_{.30}Fe_{2.40}Mn_{.02}Mg_{1.95}Si_{5.4}Al_{2.6}O_{20}(OH)_4$
Cordierite(2)	$Al_{3.00}Fe_{.79}Mn_{.05}Mg_{1.11}Si_5AlO_{18}$
Ilmenite(2)	$Fe_{1.58}Mn_{.42}Ti_2O_6$
Plagioclase(2)	$Na_{.78}Ca_{.22}Al_{1.22}Si_{2.78}O_8$

It was not possible to balance equation 2-IV using the above phase compositions without the addition of MnO to the reactants. This is a flaw in the reaction as given, arising probably from differences in the bulk compositions of the rocks from which the mineral analyses for the products and reactants were taken. Atypically high MnO contents may be characteristic of garnet-bearing rocks (discussed in Section 2.7.3). Though not as well documented as for reaction 2-III, because of the scarcity of garnet-containing samples, the ferromagnesian phases involved in reaction 2-IV are believed to systematically change to higher Mg/Mg+Fe ratios as the reaction proceeds (with increasing temperature across the cordierite + K-feldspar ± garnet zone). Therefore, equation 2-IV is again only representative of the extent to which the reaction has proceeded in the example chosen. This compositional shift in the phases (three-phase AFM field biotite-cordierite-garnet) is shown in Fig. 2-6E, using samples 64 and 391. This figure will be discussed further in Section 2.7.3.

2.6.6 Retrograde Reactions

Cordierite alteration to muscovite, chlorite, and ilmenite has been described in Section 2.4. Such retrograde assemblages are commonly associated with poorly defined rounded biotite relics, and the retrogression appears to result from the reversal of reaction 2-II.

As described in Section 2.5.6, cordierites are also seen, especially on their edges, to alter to a yellow isotropic material. From probe data on this material presented in Table 2.4, it seems to consist predominantly of Si and Al and appears to have a chemical analysis similar to that of kaolin. Its isotropic appearance may be the result of its extremely

fine grainsize. The yellowish "kaolin" may be derived from the breakdown of cordierite to chlorite, for this leaves an excess of Si and Al. However, this is not texturally supported because the retrograde breakdown of cordierite commonly involves "kaolin" as the only alteration product. Similarly the direct formation of chlorite from cordierite is unlikely, since the Mg/Mg+Fe ratio of retrograde chlorite does not coincide with that of cordierite, but lies between those of cordierite and biotite (Section 2.5.3). Therefore, retrograde reactions involving the formation of "kaolin" plus biotite are envisaged. In the lower-grade zones, the reaction is believed to be approximated by

$$\text{Cordierite} + \text{Muscovite} + H_2O \rightarrow \text{Biotite} + \text{"Kaolin"}$$

whereas in the higher-grade zones, where K-feldspar has replaced muscovite, the reaction becomes

$$\text{Cordierite} + \text{K-feldspar} + H_2O \rightarrow \text{Biotite} + \text{"Kaolin"}.$$

These reactions would involve adjustment of the prograde biotite composition, though it is feasible that the biotite reacts further with cordierite to form muscovite + chlorite as described above.

2.7 PHASE RELATIONS

2.7.1 Introduction

This section is concerned with the compositional variations shown by the phases associated with the prograde reactions described in Section 2.6. Of primary concern is the variation in Mg/Mg+Fe ratios shown by the ferromagnesian minerals. These phase relations characterise the postulated reactions as either discontinuous or continuous. Therefore, it is first appropriate to discuss the concepts of discontinuous and continuous reactions as defined by previous authors.

2.7.2 Discontinuous and Continuous Reactions

Thompson (1976a) defined discontinuous reactions as involving a distinct change in the topology of the AFM diagram, whereas continuous reactions involve continuous changes in the compositions of phases, corresponding to displacements of specific three-phase fields in an AFM diagram. However, such definitions are not sufficiently definitive of

discontinuous reactions, as continuous reactions also commonly involve distinct changes in the topology of the AFM diagram, accompanying the formation of a new phase (or phases). More explicit definitions have been given by Yardley *et al.*, (1980, p.380): (1) Discontinuous or univariant reactions lead to a change in topology of the phase diagram as a mineral or mineral pair becomes unstable at a univariant curve. (2) Continuous reactions involve coexistence of reactants and products across a temperature interval, in which they change in relative abundance and composition. Yardley *et al.*, (1980) also defined cation exchange reactions, which lead to changes in mineral compositions while their abundances remain constant, but these reactions are not considered further in this work.

Discontinuous reactions can therefore be recognised with increasing metamorphic grade by the immediate loss of a phase (or phases) in association with the formation of a new phase (or phases). Although some phases may change composition in a discontinuous reaction, these changes do not occur over a temperature interval. Conversely, all reactants and products of continuous reactions continue to coexist after a new phase has formed, until one of the reactants is exhausted or another reaction is intersected, and continuous reactions can be recognised by systematic changes in mineral chemistry as the reaction proceeds with increasing temperature.

Continuous reactions occur as a result of the consistent differences, defined by the distribution coefficients, between the Mg/Mg+Fe ratios of coexisting ferromagnesian phases. Consider an assemblage, in which A is the only ferromagnesian phase, reacting to form an assemblage containing B as the only ferromagnesian phase, and the distribution of Mg/Mg+Fe between these two phases greatly favours B. The reaction cannot take place without adjustment of the phase compositions (as Mg/Mg+Fe ratios could not be balanced on both sides of the reaction equation). Consequently phase A breaks down over a temperature interval as its stability is dependent on its composition (i.e. its Mg/Mg+Fe ratio), and both A and B are driven to more Fe-rich compositions. If all other phases in the reaction are in excess, then theoretically the reaction would proceed until phase A is exhausted and phase B has a Mg/Mg+Fe ratio equal to the original ratio of phase A (i.e. the Mg/Mg+Fe ratio of the rock). Conversely, discontinuous reactions occur with the reaction equation chemically balanced at a specific temperature. For example, if a third ferromagnesian

phase C forms with B in the above reaction, and their coexisting Mg/Mg+Fe ratios decrease in the order B → A → C, then a balanced reaction (at least with respect to Mg/Mg+Fe) can occur without a required adjustment in the phase compositions over a temperature interval.

Continuous and discontinuous reactions have been represented by Thompson (1976a,b) on isobaric T-X(Fe-Mg) diagrams. These diagrams allow the variation in Mg/Mg+Fe in coexisting phases to be portrayed in relation to the reactions taking place during progressive metamorphism. Thompson represents continuous reactions as divariant loops along which the Mg/Mg+Fe ratios of the ferromagnesian phases involved in the reaction are designated. Thompson generates discontinuous reactions by the intersection of continuous reaction loops, representing them as isotherms on the T-X(Fe-Mg) diagram, and states (Thompson, 1976a, p.410) that the Mg/Mg+Fe ratios of the ferromagnesian phases are uniquely defined by a discontinuous reaction. Further reactions (involving ferromagnesian phases) possessing characteristics typical of discontinuous reactions (i.e. the abrupt loss of a phase with increasing temperature) that are apparently not defined by the interaction of two continuous reactions are suggested by the author in this work. Discontinuous reactions of this type will be discussed with appropriate examples in the following part of this section.

2.7.3 Phase Relations in the Walcha Road Aureole

The following description relates to the schematic T-X(Fe-Mg) diagram in Fig. 2-7, adopted from the work of Thompson (1976a,b). The diagram is based on the actual Mg/Mg+Fe values recorded in the minerals; the points shown on the diagram either represent a specific analysis or an average of similar analyses. Points discussed specifically in the text are labelled with their sample number. The vertical axis (T) is broadly correlated with distance from the contact. Reactions recognised within these rocks are shown as dark lines, whereas those inferred for schematic completion of the diagram are shown lightly. The arrows give the compositional paths of the ferromagnesian minerals for a rock with a chemical composition similar to that of sample 391.

Biotite Isograd

The biotite isograd, defined by reaction 2-I, marks the incoming

Figure 2-7: Schematic T-X(Fe-Mg) diagram for low-pressure contact metamorphism of pelites. Construction of the diagram is based on Thompson (1976a,b). Reactions occurring in the contact metamorphic aureole of the Walcha Road Adamellite are shown as dark lines. The principal phases involved in the reactions are shown at the side of the diagram. The arrows represent a typical progression with increasing temperature for a whole-rock composition of sample 391 (Table 2.1). Samples specifically mentioned in the text are labelled.

Abbreviations used are quartz = Q; chlorite = Chl; muscovite = Musc; biotite = Bi; K-feldspar = K-f; garnet = Gt; cordierite = Cd; aluminium silicate = A.s; Fe oxides = FeO's; anthophyllite = Anth.

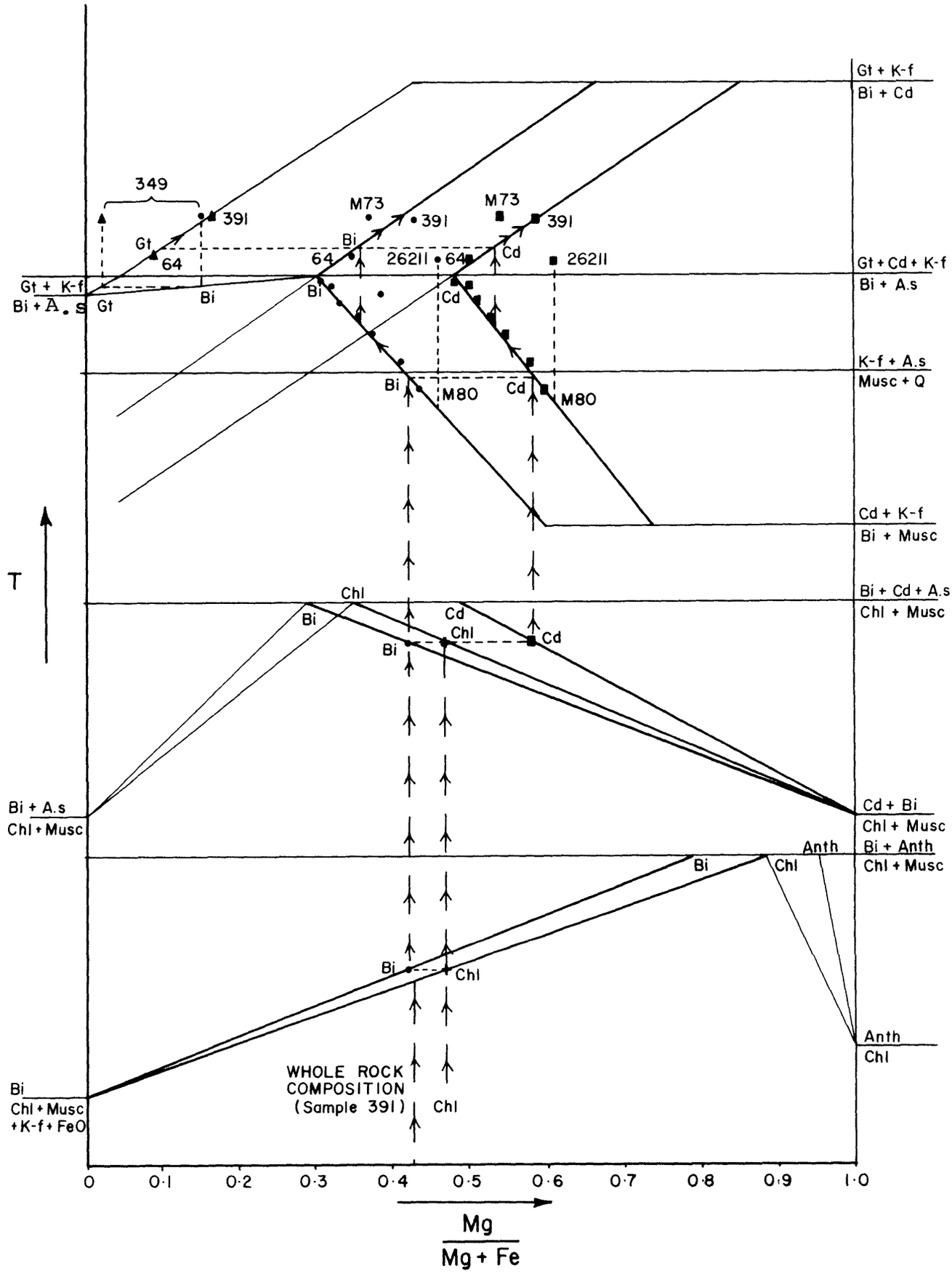
Gt + K-f
Bi + Cd
349
391
M73
391
M73
391
Gt
64
Bi
64
26211
64
Cd
26211
Gt + Cd + K-f
Bi + A.s
Gt + K-f
Bi + A.s
Gt
Bi
Bi
Cd
K-f + A.s
Musc + Q
Bi
M80
Cd
M80
Cd + K-f
Bi + Musc
T
Chl
Bi + Cd + A.s
Chl + Musc
Bi
Cd
Chl
Cd
Bi
Bi + A.s
Chl + Musc
Cd + Bi
Chl + Musc
Anth
Bi + Anth
Chl + Musc
Bi
Chl
Bi
Chl
Anth
Chl
WHOLE ROCK
COMPOSITION
(Sample 391)
Chl
Bi
Chl + Musc
+ K-f + FeO
0
0·1
0·2
0·3
0·4
0·5
0·6
0·7
0·8
0·9
1·0
Mg
Mg + Fe

of biotite and the immediate loss of K-feldspar (and possibly hematite). Therefore, this reaction is discontinuous. The discontinuous nature of this reaction has also been observed by other authors (e.g. Atherton, 1977). It is important, however, that although this reaction has discontinuous characteristics (as defined in Section 2.7.2) it is not believed to be a discontinuous reaction in the sense of Thompson (1976a), who describes discontinuous reactions as being generated by the intersection of continuous reaction loops, with the Mg/Mg+Fe ratios of the ferromagnesians being uniquely defined regardless of host-rock composition (noted above). The reason for this distinction is now briefly outlined.

No reactions have been recognised within the biotite zone above the biotite isograd, and therefore the chemistry of the phases defined at the biotite-zone boundary should be maintained throughout the biotite zone. However, biotite Mg/Mg+Fe ratios within the biotite zone are not uniquely defined, but appear to vary with host-rock chemistry (i.e. vary from sample to sample and show no systematic trends with increasing temperature; Section 2.5.5). This would not be expected if the discontinuous biotite-forming reaction occurred in the manner of discontinuous reactions outlined by Thompson (1976a).

Yardley *et al.*, (1980) also found this spread of biotite compositions within zones between reactions, and noted that it is consistent with the products of continuous reactions. This is because any particular continuous reaction can cease at different temperatures depending on the Mg/Mg+Fe ratios in the ferromagnesian phases involved, which in turn are related to host-rock composition (Yardley *et al.*, 1980, caption of Fig. 6). However, this feature does not appear to be restricted to continuous reactions, as shown by reaction 2-I. This reaction is discontinuous in character and has produced a range of biotite compositions in the biotite zone that appear to be related to the host-rock composition.

The nature of reaction 2-I is believed to be explained by the presence of Fe oxides in the pelites outside the aureole. If Fe oxides were not involved in reaction 2-I it would have to be a continuous reaction, with the Mg/Mg+Fe ratios of the biotite and chlorite changing composition along a divariant loop. The temperature at which such a reaction begins is clearly dependent on the composition of the chlorite (Atherton, 1965). The participation of Fe oxides, though, enables the reaction to be balanced (as

shown in Section 2.6.2) without requiring continuous adjustment of the phase compositions. The reaction, for any particular composition of chlorite, therefore takes place at a constant temperature and fixed Mg/Mg+Fe ratios in the ferromagnesians, until one of the reactants is exhausted. However, the temperature at which reaction 2-I (involving the Fe oxides) is initiated may still be dependent on the Mg/Mg+Fe ratio of the chlorite. If so, the relationship between the temperature of reaction 2-I and the Mg/Mg+Fe ratios of the chlorite and biotite could still be represented in a divariant loop. Hence, the discontinuous reaction for a given chlorite composition could be envisaged as occurring at a particular isotherm on the divariant loop of a T-X(Fe-Mg) diagram.

For example, consider Fig. 2-7. In the pelites outside the aureole, chlorite is the major ferromagnesian phase (phengites contain minor Fe and Mg), and the Mg/Mg+Fe ratio of the host rock (sample 391) lies to the Fe-rich side of the chlorite Mg/Mg+Fe ratio, reflecting the presence of the Fe oxides. With increasing temperature, the chlorite composition intersects the divariant loop representing the chlorite → biotite reaction (merely for schematic completion of the diagram, this loop is drawn intersecting an anthophyllite-forming reaction), and biotite is formed with a Mg/Mg+Fe ratio governed by the divariant loop (i.e. by the $K_{D(Mg)}$ value for co-existing biotite and chlorite). The temperature at which this reaction is initiated depends on the composition of the chlorite. However, owing to the participation of the Fe oxides, the reaction proceeds without continuous adjustment of the Mg/Mg+Fe ratios of the ferromagnesian phases. The reaction, therefore, takes place at constant temperature until K-feldspar (and possibly hematite) is exhausted, denoting its discontinuous nature.

Thus, reactions defined by divariant loops appear to be able to occur in a discontinuous manner at constant temperature for any particular composition of the reactants. With regard to the chlorite → biotite reaction, the temperature of reaction, and the Mg/Mg+Fe ratio of the resultant biotite, are dependent on the Mg/Mg+Fe ratio of the reactant chlorite, which in turn is determined by host-rock chemistry. This is consistent with the spread of biotite composition in the biotite zone. This type of discontinuous reaction is unlike discontinuous reactions defined by the intersection of continuous reaction loops (described by Thompson, 1976a), which occur at a specific temperature with uniquely

defined Mg/Mg+Fe ratios in the ferromagnesians regardless of host-rock composition. These two types of discontinuous reaction should be recognised as being quite distinct.

However, the type of discontinuous reaction proposed above is not unequivocal for reaction 2-I (it is more conclusively demonstrated at the cordierite isograd, discussed below), because the participation of Fe oxides could cause the reaction to take place at an isotherm, completely regardless of the chlorite's Mg/Mg+Fe ratio (but again not at uniquely defined phase compositions, as required by Thompson, 1976a). To further understand the mechanics of this reaction, experimental data on the temperatures at which Fe oxides react with end-member compositions of chlorite to form biotite, and sampling of a large variation in host-rock composition at the biotite isograd, would be required. Both these approaches could resolve whether the Mg/Mg+Fe ratios of the ferromagnesian phases involved in this reaction map out a divariant loop or an isotherm on the T-X(Fe-Mg) diagram.

Cordierite Isograd

With increasing temperature the mineralogy passes unchanged through the biotite zone (Fig. 2-7) until temperatures are reached sufficiently for the formation of cordierite by reaction 2-II. This reaction is recognised by the incoming of cordierite and the associated immediate loss of chlorite. No systematic change in the Mg/Mg+Fe ratios of either biotite or cordierite are associated with this reaction. Hence, it is a discontinuous reaction. Ramsay (1974) also noted the discontinuous nature of this reaction. However, again this is not a discontinuous reaction as recognised by Thompson (1976a), because the Mg/Mg+Fe ratios of the ferromagnesian phases are not uniquely defined. As discussed for the biotite isograd, this is denoted by the variation in the Mg/Mg+Fe ratios of the biotite throughout the cordierite zone (Section 2.5.5), even though no evidence of further reaction above the cordierite isograd exists within this zone. Indeed Thompson (1976a, Figs 1C and 2) represents the formation of biotite and cordierite from the breakdown of chlorite and muscovite as a continuous reaction loop. This divariant loop is reproduced here in Fig. 2-7, representing reaction 2-II.

No shift of the biotite and cordierite Mg/Mg+Fe ratios occur along this divariant loop in reaction 2-II, because the Mg/Mg+Fe ratio of the

Addendum to section 2.7.3 - Cordierite Isograd

Although not found in this study, Teale (1974) described and photographed andalusite in the Walcha Road aureole. Teale (pers. comm.) has stated that andalusite is rare, but from the discussion in section 2.7.3 it does denote that some iron-rich rocks do occur in the sequence. This is also confirmed by the presence of sample 349 (described on p.70).

chlorite is between those of the biotite and cordierite products (biotite increases in modal amount), allowing the reaction equation to be balanced at a specific temperature, and thus giving the reaction its discontinuous character (minor ilmenite is involved in the reaction, but this does not alter the argument). From Fig. 2-7 it is evident that the temperature at which the reaction is initiated depends on the composition of the chlorite. As implied above for the biotite isograd, this temperature dependence on chlorite composition (i.e. host-rock chemistry) would be very difficult to detect without extensive sampling (and whole-rock data) of a range of rock compositions at a given location of the zone boundary. The change in the Al/Fe+Mg ratio of the biotite across the cordierite isograd (Section 2.5.5) is analogous to muscovite becoming less phengitic with the formation of a new ferromagnesian phase at the biotite isograd.

Reaction 2-II proceeds until chlorite is exhausted. With a further increase in temperature, the Mg/Mg+Fe ratios of the biotite and cordierite remain unchanged, in rocks of any particular bulk chemistry, throughout the cordierite zone. No reaction occurs at the discontinuous reaction defined by the intersection of reaction 2-II with the biotite + Al-silicate producing reaction (shown in Fig. 2-7), because chlorite has been consumed at the earlier boundary. The lack of low-grade biotite + Al-silicate (andalusite)-containing assemblages in the Walcha Road aureole is in contrast to many studies on contact metamorphosed pelites (e.g. Compton, 1960; Okrusch, 1969). This is easily explained in terms of the T-X(Mg-Fe) diagram, because the biotite + andalusite assemblages are restricted to more Fe-rich compositions than those sampled here. The restriction of andalusite-bearing pelitic schists to Fe-rich compositions has been discussed by Labotka *et al.*, (1981, p.79).

Cordierite + K-feldspar Isograd

The incoming of K-feldspar occurs in Fig. 2-7 where the Mg/Mg+Fe ratio of the biotite intersects the divariant loop representing reaction 2-III. In contrast to the lower-grade zones, systematic compositional changes have been found in the ferromagnesians throughout the cordierite-K-feldspar zone (Fig. 2-3C; 2-4; 2-6D). This is shown in Fig. 2-7, with the biotite and cordierite Mg/Mg+Fe ratios decreasing along the divariant loop. Hence reaction 2-III is a continuous reaction. The difference between this reaction and those at the biotite and cordierite isograds is

that the newly forming phase (cordierite) lies well to the Mg side of the reactants (primarily biotite). Therefore, since the cordierite increases in modal content, both phases must become richer in Fe, as governed by the whole-rock composition of the rock. A large number of points has been located along this curve, but this is representative of the slight variation of Mg/Mg+Fe in the rocks, and a more typical shift for a given example is probably expressed by the arrows in Fig. 2-7. The temperature at which the biotite + muscovite breakdown begins is dependent on the composition of the biotite, whereas the temperature interval over which the mineral compositions change (i.e. the extent of the reaction) will depend mainly on the amount of muscovite available. Loss of muscovite ends the reaction, and with increasing temperature the Mg/Mg+Fe ratios of the cordierite and biotite will no longer vary along the divariant loop, but remain fixed at the compositions where the reaction ceased (or become "frozen-in" as coined by Yardley *et al.*, 1980). That is, the mineral composition paths leave the divariant loop as shown in Fig. 2-7.

Though reaction 2-III involves the breakdown of muscovite with biotite, the breakdown of muscovite plus quartz to K-feldspar and Al-silicate lies at temperatures only slightly above the beginning of the former reaction (see Section 2.9). At temperatures above the muscovite + quartz breakdown, reaction 2-III becomes

$$\text{Biotite} + \text{Al-silicate} \rightarrow \text{Cordierite} + \text{K-feldspar} + H_2O$$

(e.g. Thompson, 1976a, Fig. 2B). Hence the assemblage biotite + muscovite + cordierite + K-feldspar, present in the outer part of the cordierite + K-feldspar zone (sample M80), is unstable at higher grades, and therefore the muscovite in sample M78, midway through this zone, may represent retrogressed Al-silicate (andalusite or sillimanite), explaining its unusual textural appearance (Section 2.4.4). The rarity of Al-silicates or muscovite in the cordierite + K-feldspar + biotite assemblages, though, suggests that the higher temperatures of this zone have been sufficient to consume these phases, and that the close fit of points with the divariant curves may be more schematic than real.

Garnet Isograd

Cordierites and biotites from samples near the contact have higher Mg/Mg+Fe ratios than those from the inner part of the cordierite + K-feldspar zone (Section 2.5). For garnet-containing rocks this is clearly understood

from the continuous nature of reaction 2-IV shown in Fig. 2-7. The garnet is far richer in Fe than the reacting phases, cordierite and biotite. Therefore, as garnet increases in modal amount, all the ferromagnesian minerals, including garnet, must change to more Mg-rich compositions. Though sample 64 was not found in the Walcha Road aureole, but from the southern contact of the Mt Duval Adamellite, it has been included as an example of an Fe-rich garnet-bearing rock. It contains cordierite, biotite, garnet and K-feldspar in apparent equilibrium, and is therefore believed to lie on the continuous reaction loop representing reaction 2-IV. If so, it represents a lower temperature of equilibration than does sample 391. The shift in composition with increased temperature from sample 64 to 391, has also been represented in Fig. 2-6E (AFM diagram).

From Fig. 2-7 it is evident that the richer the cordierite and biotite are in Mg, the higher are the temperatures required to form garnet from reaction 2-IV. Sample 26211 (lacking garnet) appears to be a sample which, although within the cordierite + K-feldspar ± garnet zone (30 metres from the contact), has too high a Mg/Mg+Fe ratio (high Mg/Mg+Fe ratios of cordierite and biotite) to allow garnet to form (Figs. 2-6E and 2-7). Hence the sporadic occurrence of garnet in the innermost zone of the Walcha Road Adamellite is believed to be related to insufficient temperatures, even at the contact, to form garnet unless the rocks are Fe rich. The proposed restricted occurrence of garnet in this aureole to the more Fe-rich rocks is consistent with the findings of Chinner (1962). However, this does not appear to be the only compositional criterion controlling garnet formation. Sample M73 (Fig. 2-7), collected at the contact, contains biotite and cordierite richer in Fe than those found in sample 391 (Fig. 2-6E), but does not contain garnet. It is suggested that the Mn content (and possibly the Ca content) of the rocks plays a major role in stabilising the garnet at lower temperatures. From Table 2.1 the two garnet-containing rocks (64 and 391) do have higher Mn values. The increased stability of Mn-rich garnets has been noted by several authors (e.g. Hsu, 1968; Okrusch, 1971; Weisbrod, 1973; Blumel and Schreyer, 1977). **Teale (1974) also suggested that fo_2 may affect garnet stability.**

Sample 349, containing extremely Fe-rich garnets and biotites (Fig. 2-6E), is notable within the garnet zone. This is very iron-rich rock, and garnet has formed by the reaction

$$\text{Biotite} + \text{Al-silicate} \rightarrow \text{Garnet} + \text{K-feldspar} + H_2O$$

(Fig. 2-7) rather than by reaction 2-IV. This reaction intersects reaction 2-III to give the discontinuous reaction

$$\text{Biotite} + \text{Al-silicate} \rightarrow \text{Garnet} + \text{Cordierite} + \text{K-feldspar} + H_2O$$

(Thompson, 1976a, Fig. 2B). Mg/Mg+Fe ratios of the biotite and cordierite in sample 349 are fixed when Al-silicate is exhausted in the reaction, and these ratios remain as temperature increases (Fig. 2-7).

2.7.4 Distribution Coefficients

The distribution coefficient (K_D) of Mg for coexisting biotite (Bi) and cordierite (Cd) is defined by

$$K_{D(Mg)}^{Bi-Cd} = \frac{X_{Mg}^{Bi}}{1-X_{Mg}^{Bi}} \cdot \frac{1-X_{Mg}^{Cd}}{X_{Mg}^{Cd}}$$

where X_{Mg} represents the Mg/Mg+Fe atomic ratio in the biotite and cordierite. $K_{D(Mg)}^{Bi-Cd}$ values decrease systematically with increasing grade throughout the cordierite + K-feldspar zone. This may be related to temperature, giving the "tie-line rotation" discussed by Thompson (1976a, p.420). However, $K_{D(Mg)}^{Bi-Cd}$ appears to be related to the Mg/Mg+Fe ratio of the biotite rather than temperature, as an excellent correlation occurs between $K_{D(Mg)}^{Bi-Cd}$ and X_{Mg}^{Bi} in biotite + cordierite + K-feldspar assemblages (Fig. 2-8), including the garnet-free samples from the innermost zone (i.e. samples 26211 and M73). Conversely, biotite-cordierite pairs associated with either chlorite, in the cordierite zone, or garnet, in the cordierite + K-feldspar ± garnet zone, lie well above the general trend shown in Fig. 2-8. This implies that mixing within the phases is not ideal, with $K_{D(Mg)}^{Bi-Cd}$ values being affected by the presence of other ferromagnesian phases, and by the Mg/Mg+Fe ratio of the biotite. Distribution coefficients for biotite and garnet, and cordierite and garnet, were also examined in the few available samples. Very similar values occur in samples 64 and 391, with $K_{D(Mg)}^{Bi-Gt}$ values between 4.0 and 4.5, and $K_{D(Mg)}^{Cd-Gt}$ values of 7.8 and 7.9 respectively. But, the Fe-rich sample (349), which does not contain cordierite, has a much higher $K_{D(Mg)}^{Bi-Gt}$ value of 9.0. This implies that the $K_{D(Mg)}^{Bi-Gt}$ values are affected by the presence of cordierite, and again mixing does not appear to be ideal.

Figure 2-8: Mg-Fe distribution coefficient for biotite and cordierite ($K_{D(Mg)}^{Bi-Cd}$) versus the Mg/Mg+Fe ratio of biotite (X_{Mg}^{Bi}).

Symbols:
- ▲ cordierite zone
- ● cordierite + K-feldspar zone
- ■ gt-bearing rocks of the cordierite + K-feldspar ± garnet zone
- □ gt-absent rocks of the cordierite + K-feldspar ± garnet zone

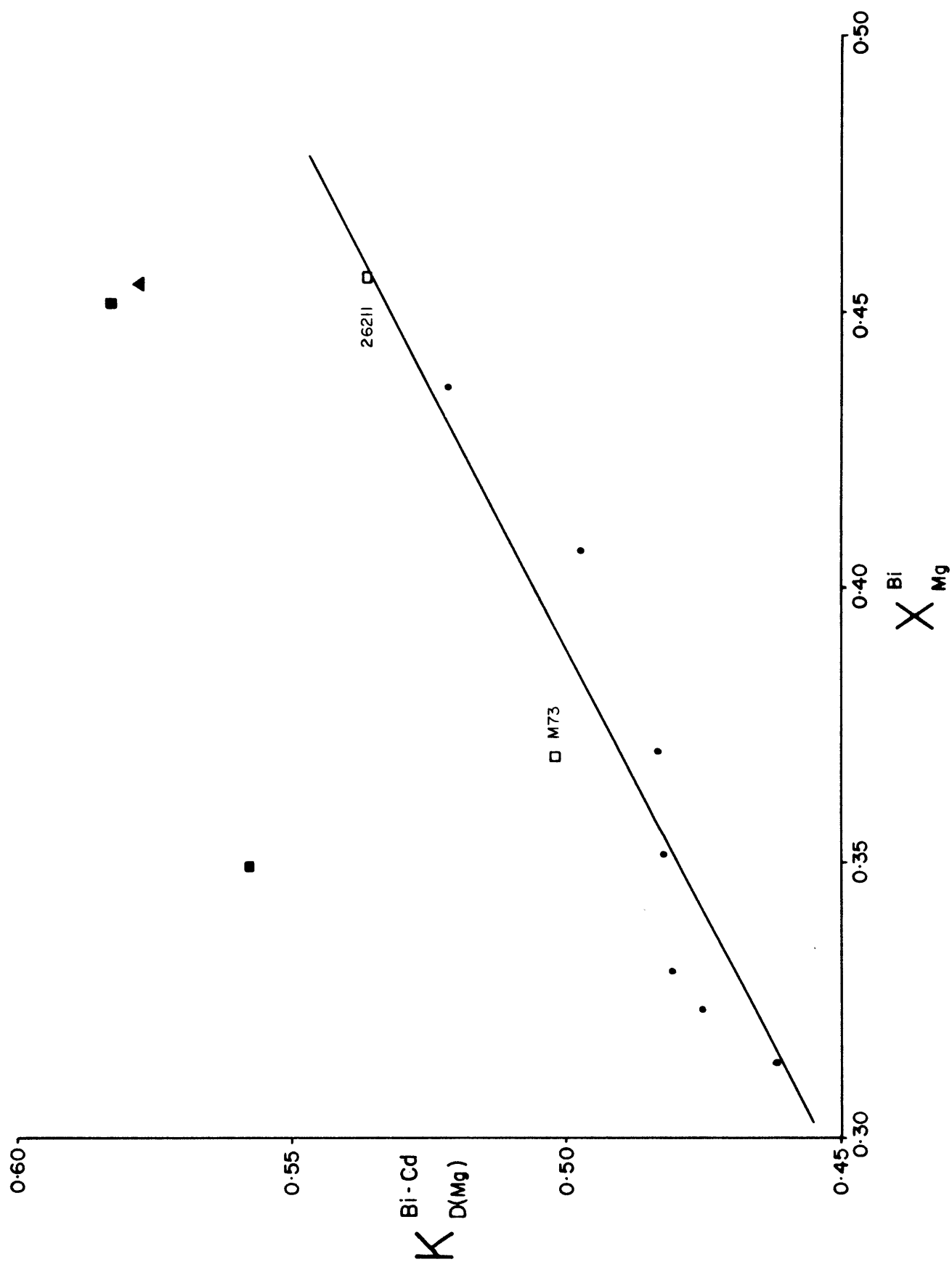
0·60
0·55
0·50
0·45
0·30
0·35
0·40
0·45
0·50
$K_{D(Mg)}^{Bi-Cd}$
X_{Mg}^{Bi}
26211
M73

2.7.5 Summary of Conclusions

Progressive metamorphism of the Walcha Road aureole can be represented on a T-X(Fe-Mg) diagram by reactions occurring on divariant reaction loops (though, the actual nature of the biotite-forming reaction is uncertain). Discontinuous reactions generated by the intersection of continuous reactions (represented as isotherms, Thompson, 1976a) have not been recognised, apparently as consumption of one of the reacting phases (be it a ferromagnesian mineral or not) occurs on the divariant loops before discontinuous reactions of this type are reached. These conclusions agree with those reached by Yardley *et al.* (1980, p.385) describing regionally metamorphosed Fe-rich pelites. However, both discontinuous and continuous types of reactions are still discernible within the series of reactions. The two inner zone boundaries are defined by continuous reactions, which proceed over a temperature interval with the ferromagnesian phases changing composition along the divariant loop, whereas the two outer zone boundaries are defined by discontinuous reactions, which proceed at a constant temperature associated with the immediate loss of at least one of the reacting phases.

Reactions occurring on divariant loops are generally not considered appropriate for defining isograds, because their initiation is dependent on host-rock composition. However, provided the variation in host-rock chemistry (primarily Mg/Mg+Fe) is not too large, consistent temperature-related zones can be defined, and temperatures may be assigned to the zone-boundary reactions if experimental data have been determined on ferromagnesian compositions similar to those occurring in the rocks studied (see Section 2.9).

2.8 MIGMATITE PETROGENESIS

Four hypotheses are generally put forward to explain the origin of migmatites (as discussed by White, 1966; Amit and Eyal, 1976; and Yardley, 1978). These hypotheses are: 1) injection: the injection of igneous magma into country rock; 2) metasomatism (external metasomatism, Yardley, 1978): the introduction of material by diffusion or infiltration into a rock from an external source; 3) anatexis: the formation of low-temperature melts by partial melting of the country rock; 4) meta-

morphic segregation: the formation of felsic veins by the segregation of locally derived material without melting. The first two processes involve the introduction of material from an outside source, whereas the last two involve no change in the bulk composition of the migmatised rock (commonly referred to as formation *in situ*).

The petrography of the migmatites has been described in Section 2.4. From Table 2.1 an analysis of sample 391, a thinly veined migmatite, is seen to lie within the range of compositions of the interlayered pelitic and quartzo-feldspathic sediments. This is not conclusive, but possibly suggests that the bulk chemical composition of the country rocks may not have been altered during migmatisation. Also, several features within these migmatites (Section 2.4) are very similar to those described in migmatites by other authors to discount the possibility of the veins forming by the introduction of external material. These include the lack of sharp planar boundaries on the veins and the occurrence of distinct biotite-rich selvedges (Plate 2-2D).

Plagioclase grains from the felsic veins, selvedges, and matrix of sample 391 are chemically identical (Table 2.6). Similarly, biotites occurring within the veins are, allowing for their inherently greater range of composition, very similar chemically to biotites within the selvedges and surrounding host rock (Table 2.6). This compositional similarity between minerals in the veins and selvedges and those in the host is good evidence for *in situ* formation of the migmatites.

In comparison with the mineralogy of the adjacent pluton, compositions of biotites from felsic veins in sample 391 are distinct from those of biotites recorded from the southeast edge of the Walcha Road Adamellite (Table 2.6). Biotites from the pluton have higher Ti contents and Mg/Mg+Fe ratios, and significantly lower Al^{VI} contents than those in the felsic veins of sample 391. This tends to suggest that the vein material does not represent injected magma from the Walcha Road Adamellite.

The following discussion is mainly concerned with differentiating between the *in situ* possibilities of metamorphic segregation and partial melting. Because petrographic features are typically ambiguous with regard to these possibilities, this discussion is based primarily on chemical evidence concerned with modal plots on the Qz-Ab-Or-An-H_2O diagram (Winkler,

TABLE 2.6. Biotite and plagioclase analyses from the migmatised sample 391 and the Walcha Road Adamellite

	BIOTITE							PLAGIOCLASE			
	391	391	391[x]	391	389B*	G8*		391	391	391	391
	host	host	selvedge	felsic vein	igneous	igneous		host	host	selvedge	felsic vein
SiO_2	35.27	34.19	34.20	34.90	36.16	37.59		61.51	60.39	61.72	61.35
TiO_2	2.64	1.69	2.27	2.36	4.15	3.43		-	-	-	-
Al_2O_3	20.21	20.49	19.80	19.48	13.93	13.97		24.67	24.60	24.66	24.78
FeO**	18.39	18.24	19.19	19.23	18.57	18.24		-	-	0.15	-
MnO	0.15	0.15	0.26	0.15	-	0.25		-	-	-	-
MgO	7.91	8.37	8.86	8.71	11.38	13.02		-			
CaO	0.11	-	0.10	-	-	0.20		5.57	5.49	5.43	5.53
Na_2O	0.23	0.33	0.20	0.20	-	0.18		8.11	8.22	8.28	8.24
K_2O	9.81	9.65	9.42	9.75	9.70	9.01		0.13	0.35	0.16	0.30
Total	94.72	93.11	94.30	94.78	93.89	95.89		99.99	99.05	100.40	100.20
Structural formulae[÷]											
Si	5.383	5.316	5.276	5.354	5.607	5.663		10.902	10.836	10.905	10.870
Al^{IV}	2.617	2.684	2.724	2.646	2.393	2.337		5.156	5.205	5.138	5.177
Al^{VI}	1.021	1.074	0.879	0.879	0.155	0.143					
Ti	0.303	0.198	0.263	0.272	0.484	0.389		-	-	-	-
Fe^{2+}	2.347	2.372	2.476	2.467	2.408	2.298		-	-	0.022	-
Mn	0.019	0.020	0.034	0.020	-	0.032		-	-	-	-
Mg	1.799	1.940	2.037	1.991	2.630	2.923					
Ca	0.018	-	0.017	-	-	0.032		1.058	1.055	1.028	1.050
Na	0.068	0.100	0.060	0.060	-	0.053		2.787	2.860	2.837	2.831
K	1.910	1.914	1.854	1.908	1.919	1.731		0.030	0.080	0.036	0.068
Total Cations	15.485	15.618	15.619	15.597	15.596	15.600		19.933	20.036	19.966	19.996
Mg/Mg+Fe	0.434	0.450	0.451	0.447	0.522	0.560	Or	0.76	2.01	0.92	1.72
Ti/Sum Y	0.055	0.035	0.046	0.048	0.085	0.067	Ab	71.94	71.58	72.72	71.69
							An	27.30	26.42	26.35	26.59

x The biotite analysis from sample 391 in Table 4.2 is also from a selvedge

* Biotite analyses from the southeast margin of the Walcha Road Adamellite; G8 from Flood (1971)

÷ Biotite based on 22 oxygens, plagioclase based on 32 oxygens

** Total Fe as FeO

1976). Modal analysis of the thin felsic veins (e.g. sample 391) proved to be impracticable because they were too intimately intermingled with their surrounding material to give reliable results. Therefore, modal analyses were taken from the wider and coarser-grained felsic veins and patches (intermediate to the leucocratic lenses) described from the migmatites of locality M6 (Section 2.4.6) (i.e. M6F, three analyses). A modal analysis has also been taken from a felsic dyke (M5) associated with the migmatised sediments. The dyke is texturally and mineralogically identical to the felsic veins, and is believed to have a similar origin (Section 2.4.6).

Qz-Or-Ab-An proportions, calculated from these modes, and microprobe feldspar analyses (Table 2.7) are plotted on the Qz-Or-Ab-An-H_2O diagrams for 1 and 2 Kb P_{H_2O} in Fig. 2-9. The cotectic curves are based on data from James and Hamilton (1969) for 1 Kb and von Platen (1965) for 2 Kb. In Fig. 2-9, the felsic material plots very close to the cotectic curves for 1 and 2 Kb. Combined with the earlier evidence for *in situ* formation, this is consistent with an anatectic origin (at least for the felsic material analysed). From the An contents in Fig. 2-9 it is possible that sample M5 (a felsic dyke) fits more closely to the cotectic curve for 2 Kb, whereas the plots for M6F lie closely around the 1 Kb curve. Therefore, it is tentatively suggested that the dykes may represent material which has formed at slightly greater depth, and has completely separated from its source material.

The felsic compositions plotted in Fig. 2-9 are inconsistent with compositions of vapour phases associated with granitic magmas at low pressures for the latter are very rich in silica (Luth and Tuttle, 1968). Only above 10 Kb P_{H_2O} do vapour phase compositions in equilibrium with minimum melts even approximately coincide with the cotectic curves for the beginning of melting. Hence, this is evidence against such an origin for the felsic material in the migmatites and the associated felsic dyke.

Field relations (Section 2.4.6) are consistent with an anatectic origin for the migmatites. The migmatised (veined) sediments grade into the leucocratic lenses (Section 2.4.6), and the intense folding and disrupted nature of the migmatised sediments is typical of rocks which have lost their competence because of the onset of melting within them. Such morphology is not expected with metamorphic segregation (Yardley, 1978). Plagioclase compositions have also been used by previous authors

TABLE 2.7. Modal analyses of the leucocratic material plotted in Fig. 2-9

	Modal proportions			Calculated molecular proportions				
	Quartz	K-feldspar	Plagioclase	Qz	Or	Ab	An	
M6F.1	44.58	36.31	19.11	44.58	33.63	17.47	4.32	*
				46.59	35.15	18.26		†
M6F.2	35.33	39.05	25.62	35.33	36.23	22.66	5.78	
				37.50	38.45	24.05		
M6F.3	37.73	39.25	23.02	37.73	36.38	20.69	5.20	
				39.80	38.38	21.82		
M5	38.32	31.35	30.33	38.32	29.01	26.58	6.09	
				40.81	30.89	28.30		

M6F : felsic vein in migmatite
M5 : felsic dyke intruding migmatite
Samples are discussed in the text, Sections 2.4.6 and located in Fig. 2-1C.

Modal analyses derived by point counting thin sections stained with Na cobaltinitrite

Qz-Or-Ab-An values based on microprobe feldspar analyses:

		An	Ab	An
M6F	K-feldspar	92.06	7.94	-
	Plagioclase	1.09	76.33	22.58
M5	K-feldspar	91.37	8.63	-
	Plagioclase	1.21	78.71	20.08

* Qz+Or+Ab+An = 100

† Qz+Or+Ab = 100

Differences between volume and molecular proportions are negligible and ignored.

Figure 2-9: Cotectic lines at 1 and 2 Kb P_{H_2O} for the Qz-Ab-Or-An tetrahedron projected from the An apex onto the Qz-Ab-Or face. Points along the cotectic lines represent experimentally determined melts at specific compositions (piercing points). The diagram is based on Winkler (1976). Experimental data for the curves are from James and Hamilton (1969) for 1 Kb and von Platen (1965) for 2 Kb.

Symbols:
- • piercing points
- + felsic vein in migmatite (see text)
- × felsic dyke intruding migmatite (see text)

Numbers associated with the above symbols are An contents determined on the basis of Qz+Ab+Or+An = 100. Bracketed numbers are temperatures (^{o}C) appropriate to the piercing points.

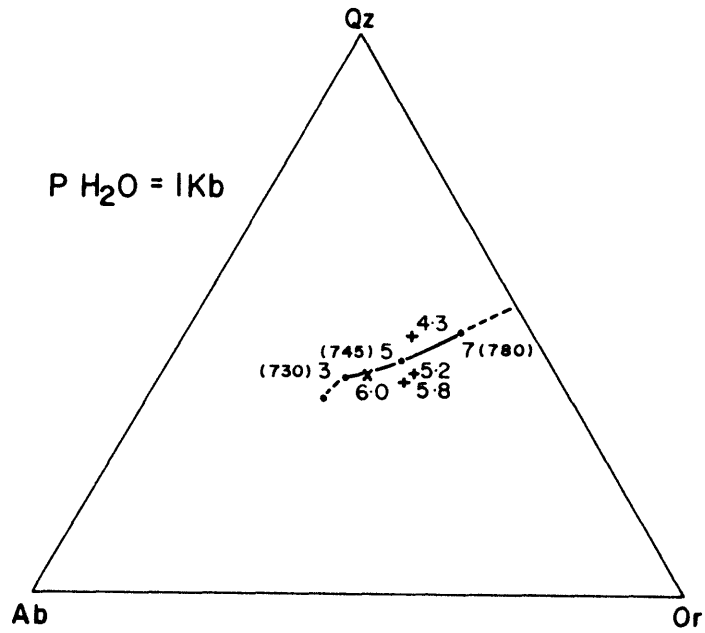
Qz
P H2O = 1Kb
4·3
(745) 5
7(780)
(730) 3
5·2
6·0
5·8
Ab
Or

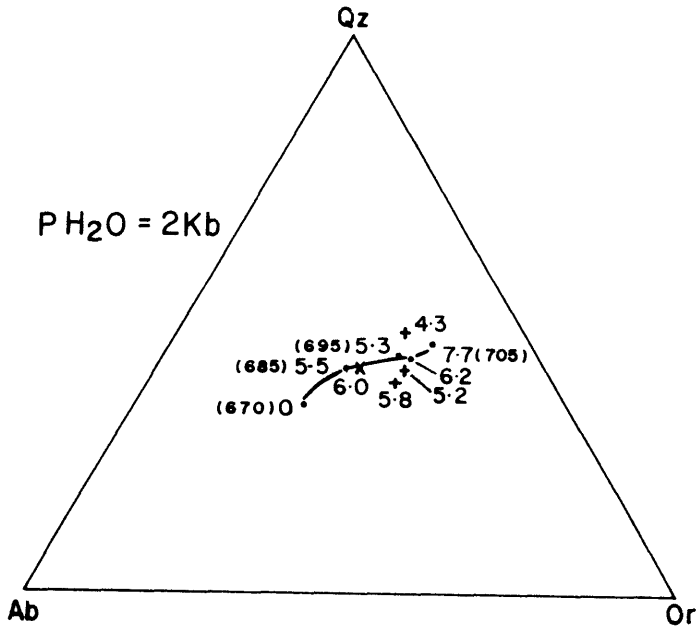
Qz
P H2O = 2Kb
4·3
(695) 5·3
7·7(705)
(685) 5·5
6·2
6·0
5·8
5·2
(670) 0
Ab
Or

(e.g. Vernon, 1976) to differentiate between metamorphic segregation and partial melting; the albite component of plagioclase should be preferentially fractionated into the melt phase. In the well separated leucosome material the plagioclase does appear to be more albitic (Ab 78) compared with the granoblastic plagioclase of the associated metasediment (Ab 72). But, in the more thinly veined migmatite (sample 391) identical plagioclase analyses have been recorded from grains within the leucosome, melanosome and palaeosome, as noted previously. This may imply metamorphic segregation for this veining. However, the determinative use of plagioclase compositions is ambiguous, as discussed by Ashworth (1976,1977) and Yardley (1977). Similarly, plagioclase analysed from within the leucosome veins may well be restite, since much restite is clearly present amongst these veins (biotite and polygonal aggregates of quartz and feldspar). Finally, the retrograde alteration that is abundant in (and often restricted to) the leucocratic veins and more-thoroughly migmatised rocks, and the occurrence of tourmaline within the felsic veins, have both been attributed by Ashworth (1976, p.677) to the presence of a melt.

Although the above evidence is not conclusive, it certainly appears that *in situ* melting has been responsible for development of the migmatites. The melts would be derived from the quartz-plagioclase-K-feldspar portion of the high-grade rocks, with the large K-feldspar component being formed by the higher-grade reactions 2-III and 2-IV. However, this does not deny the possibility of vein formation by metamorphic segregation at temperatures below those of melting. Indeed this could promote felsic layers which are chemically more likely to subsequently undergo melting.

2.9 P-T CONDITIONS

The relevant reactions for defining the P-T conditions of contact metamorphism within the Walcha Road aureole are given in Fig. 2-10. Most experimental work for the appropriate reactions has involved the pure Mg system (e.g. Schreyer and Seifert, 1969; Seifert, 1970,1976). These reactions are denoted by the presence of either phlogopite or Mg-garnet, and in Fig. 2-10 intersections between these curves define the invariant points PIA, PIIA, and PIIIA. However, Hoffer (1978) has presented reactions defining the invariant point PII (his P2) based on Mg/Mg+Fe values of 0.50 for biotite and 0.66 for cordierite. These reactions are far more applicable

Figure 2-10: P-T diagram showing univariant reactions relevant to the contact metamorphism of pelites. Reactions involving pure-Mg phases are shown as dashed lines associated with the invariant points PIA, PIIA, PIIIA. Curves involving Fe solid solution in the phases (more appropriate to the rocks within this study, see text) are shown as solid lines intersecting at the invariant points PI, PII, and PIII.

Experimentally determined curves are labelled by circled numbers (listed below). The other curves are based on reconstructions around the invariant points PIII and PIIIA taken from Thompson (1976b, Fig.4) and Holdaway and Lee (1977, Fig.7A). The latter curves are shown as thinner lines.

Abbreviations used are quartz = Q; albite = Ab; K-feldspar = K-f; chlorite = Chl; muscovite = Musc; biotite = Bi; phlogopite = Phl; stilpnomelane = Stilp; cordierite = Cord; garnet = Gt; aluminium silicate = A.s.

Experimentally determined curves:

1. Q+Ab+K-f → Melt Tuttle and Bowen (1958) and Merrill *et al.* (1970)
2. Musc+Q → K-f+A.s Chatterjee and Johannes (1974)
3. Aluminium-silicate polymorphs Holdaway (1971)
4. Musc+Phl+Q → Cord+K-f+H_2O Seifert (1976)
5. Musc+Chl+Q → Cord+Phl+H_2O Seifert (1970)
6. Cord+Musc → Phl+A.s+Q+H_2O Schreyer & Seifert (1969)
7. Phl+A.s+Q → Cord+K-f+H_2O Schreyer & Seifert (1969)
8. Musc+Bi+Q → Cord+K-f+H_2O Hoffer (1978)
9. Cord+Musc → Bi+A.s+Q+H_2O Hoffer (1978)
10. Bi+A.s+Q → Cord+K-f+H_2O Hoffer (1978,1976)
11. Bi+Cord+Q → Gt(Fe)+K-f+H_2O Thompson (1976b)
12. Stilp+Musc → Bi+Chl+Q+H_2O Nitsch (1970)

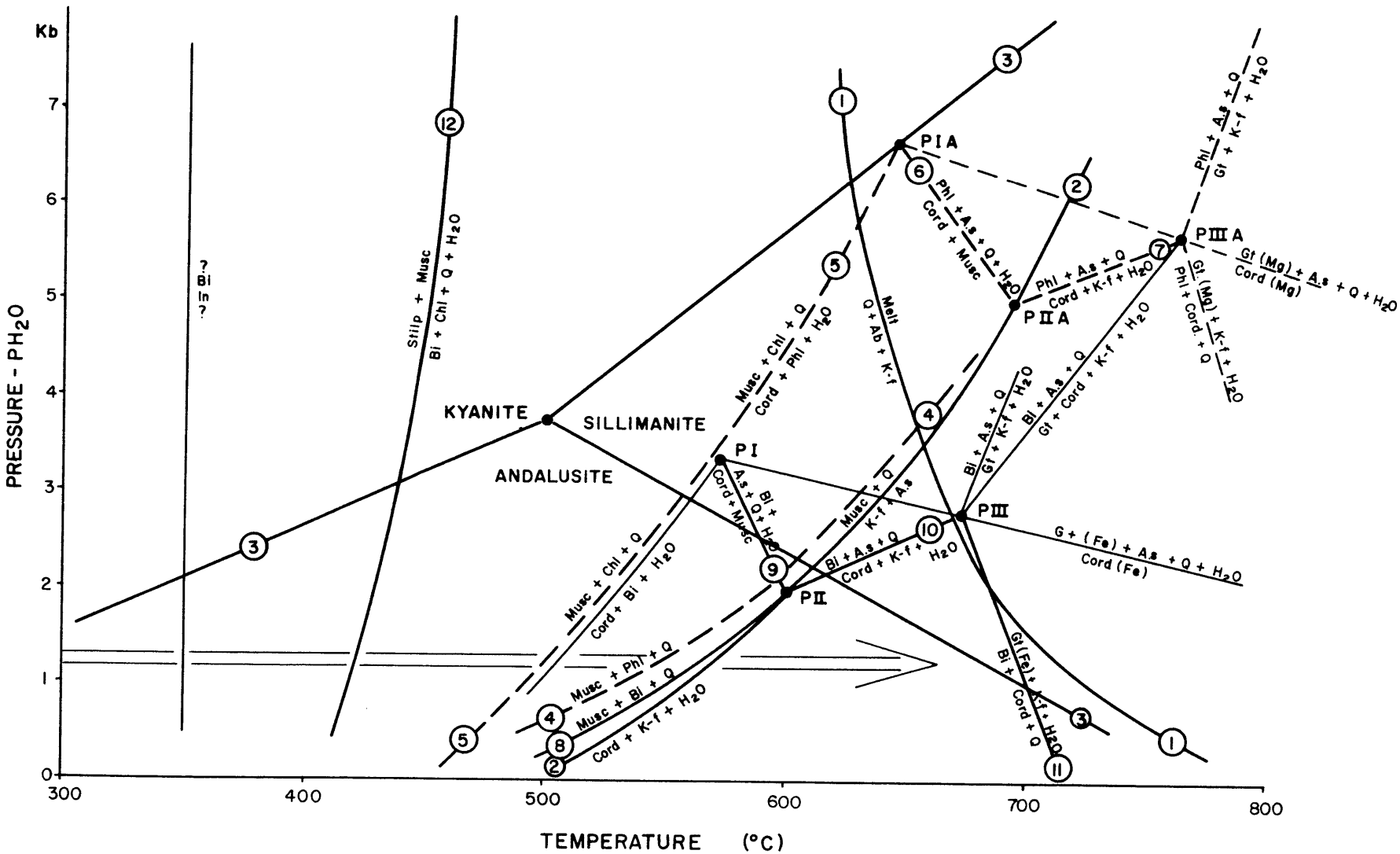
Kb
PRESSURE - PH_2O
TEMPERATURE (°C)
300
400
500
600
700
800
0
1
2
3
4
5
6
7
KYANITE
SILLIMANITE
ANDALUSITE
PI
PIA
PIIA
PII
PIII
PIIIA
Stilp + Musc
Bi + Chl + Q + H_2O
Musc + Chl + Q
Cord + Phl + H_2O
Musc + Chl + Q
Cord + Bi + H_2O
Cord + Musc
Bi + As + Q + H_2O
Musc + Phl + Q
Musc + Bi + Q
Cord + K-f + H_2O
Melt
Q + Ab + K-f
Musc + Q
K-f + As
Phl + Cord + Musc
Phl + As + Q + H_2O
Cord + K-f + H_2O
Bi + As + Q
Gt + K-f + H_2O
Gt + Cord + K-f + H_2O
Phl + As + Q
Gt + K-f + H_2O
Gt (Mg) + As + Q + H_2O
Cord (Mg)
Gt (Mg) + K-f + H_2O
Phl + Cord + Q
G + (Fe) + As + Q + H_2O
Cord (Fe)
Bi + As + Q
Cord + K-f + H_2O
Gt (Fe) + K-f + H_2O
Bi + Cord + Q

to the rocks of this study (which have Mg/Mg+Fe ratios ≈0.42 for biotite and 0.58 for cordierite in the cordierite zone). Hoffer's reactions are basically the same as those around PIIA except that biotite is involved rather than phlogopite. It is clear that with an increase in Fe in the ferromagnesian phases the position of PII shifts to lower pressures and temperatures, as do its associated univariant curves and other invariant points. This was shown by Holdaway and Lee (1977, Fig. 7A).

The construction of univariant curves around PI and PIII is based on the schematic P-T diagram of Thompson (1976b, Fig. 4), while the join PIII to PIIIA is based on Holdaway and Lee (1977, Fig. 7A) and represents the discontinuous reaction

Biotite + Al-silicate + Quartz → Garnet + Cordierite + K-feldspar + H_2O

formed by the intersection of the continuous reactions

Biotite + Al-silicate + Quartz → Cordierite + K-feldspar + H_2O and
Biotite + Al-silicate + Quartz → Garnet + K-feldspar + H_2O

(this intersection is also shown in Fig. 2-7 of this study).

The location of PIII, though, is uncertain in this diagram. Holdaway and Lee (1977) have presented data on this invariant point for various cordierite compositions, but their results give pressures and temperatures too high to be consistent with the formation of garnet within the Walcha Road aureole. It is suggested, therefore, that the location of PIII (represented by the intersection of several reactions involving garnet) varies substantially with the spessartite + grossularite content of the garnet. The results of Holdaway and Lee (1977) are based on garnets with 7 mole-% spessartite + grossularite, whereas the garnets formed in the Walcha Road aureole contain over 15 mole-% spessartite + grossularite (Table 2.2). As experimental data are not available relating the types of reactions of Holdaway and Lee (1977) (allowing for solid solution in the ferromagnesians) to variation in the spessartite + grossularite content of the garnet, then reactions involving garnet in Fig. 2-10 can be considered as only schematic. For this schematic completion, reaction 12, the Fe reaction for

Biotite + Cordierite + Quartz → Garnet + K-feldspar + H_2O

(Thompson, 1976b, Fig. 3), is used to locate PIII (Fig. 2-10). The

melting curve of Tuttle and Bowen (1958) is shown in Fig. 2-10, however, the An content of plagioclase will shift this curve to slightly higher temperatures (Winkler, 1976).

Since cordierite and K-feldspar coexist below the breakdown temperatures of

$$\text{Muscovite} + \text{Quartz} \rightarrow \text{Al-silicate} + \text{K-feldspar} + H_2O$$

the position of PII is an excellent pressure indicator. Pressures must have been below 2 Kb, and since the rocks are more Fe rich than those studied by Hoffer (1978), pressures significantly below 2 Kb would be expected. Pressures of 1 Kb (possibly 1-2 Kb) are indicated for partial melting within the migmatites (Fig. 2-9). Pressures much below 1 Kb would not be expected, as the temperatures required to begin melting at the contact become unreasonably high as pressure decreases. Therefore, pressures of 1-1½ Kb are estimated for the Walcha Road aureole.

2.9.1 Biotite Isograd

Not many experimental data are available on the formation of biotite. Temperatures of 300-400°C are often suggested for pressures of a few kilobars (e.g. Turner, 1980). In agreement with such temperatures, Pinsent and Smith (1975) have delineated temperatures of 350-370°C for the biotite isograd based on carbonate geothermometry in carbonate-bearing pelitic rocks. Katagas (1980) used the stilpnomelane plus muscovite breakdown reaction of Nitsch (1970) to represent the P-T conditions of biotite formation, since Winkler (1976) noted that this often coincides with the chlorite-biotite zone boundary. This latter reaction is presented in Fig. 2-10 as a possible maximum temperature for the biotite isograd.

2.9.2 Cordierite Isograd

The formation of cordierite with biotite by reaction 2-II (Section 2.7) is compositionally dependent, but, as noted by Winkler (1976), varying Mg/Mg+Fe ratios do not appear to greatly alter the reaction temperatures. Therefore, from Fig. 2-10, temperatures around 500-510°C are expected for pressures of 1-1½ Kb.

2.9.3 Cordierite + K-feldspar Isograd

Composition has a clear effect on the incoming of cordierite + K-feldspar, with the Mg reaction (4, Fig. 2-10) occurring 20°C below the biotite reaction (8, Fig. 2-10), as given by Hoffer (1978). Temperatures for the cordierite+K-feldspar isograd in the Walcha Road aureole (500m from the contact) are estimated at about 560°C. The continuous nature of this reaction (Section 2.7.3) causes progressively lower Mg/Mg+Fe ratios in the ferromagnesian phases with increasing temperature. This immediately alters the appearance of the P-T diagram, with PII shifting to lower pressures. Should PII fall below the proposed pressure of 1-1½ Kb within the aureole then reaction 10:

Biotite + Al-silicate + Quartz → Cordierite + K-feldspar + H_2O

will occur. In relatively Fe-rich rocks reaction 8 may not be intersected at all, for PII may initially lie below the pressures experienced in the aureole.

2.9.4 Contact Temperatures

At the pluton contact, temperatures sufficient to initiate melting in the pelites are required. From James and Hamilton (1969) the minimum melt temperature at 1 Kb for a melt with an An content of 5% (Fig. 2-9) is approximately 745°C. Even for pressures of 1½ Kb, temperatures of around 720°C would be required to form these melts. As noted above, temperatures for the garnet-forming reactions cannot be estimated accurately. However, it is evident from the construction of Fig. 2-10 that garnet formation (via the reaction

Biotite + Cordierite + Quartz → Garnet + K-feldspar + H_2O,

of which reaction 12 is an example) would be restricted to more Fe-rich rocks in close proximity to the contact (typically in rocks showing migmatisation).

2.10 SUMMARY

A sequence of interlayered pelitic and semi-pelitic sediments has been investigated in the Walcha Road aureole. Outside the aureole these sediments have been affected by very low-grade regional metamorphism,

producing muscovite + chlorite-bearing assemblages. Four metamorphic zones have been identified within the 4 km aureole:

I) Biotite zone (4 km - 1500 m);
II) Cordierite zone (1500 m - 500 m);
III) Cordierite + K-feldspar zone (500 m - 100 m);
IV) Cordierite + K-feldspar ± Garnet zone (100 m - contact).

Textural changes occur throughout the aureole, associated with the progressive development of a strong foliation parallel to the contact, and culminating in gneissic banding in the cordierite + K-feldspar ± garnet zone.

Metamorphism has proceeded via a series of discontinuous and continuous reactions which define the zone boundaries. These reactions have been delineated by the use of modal data and microprobe analyses of the minerals involved. The discontinuous reactions are characterised by the immediate loss of a reactant associated with the incoming of a new phase (i.e. reactions proceed at a constant temperature until one of the reactants is exhausted). Continuous reactions are characterised by the coexistence of reactants and products over a temperature interval associated with the systematic change in mineral abundance and chemistry.

In the Walcha Road aureole the two outer zone boundaries are represented by discontinuous reactions, whereas the two higher-grade zone boundaries are marked by continuous reactions. These reactions have been represented on a T-X(Fe-Mg) diagram. Though the exact nature of the biotite-forming reaction is questionable, it appears that both the continuous and discontinuous reactions can be represented on divariant loops, with the consequence that the temperatures of initiation of both these types of reactions are dependent on the mineral chemistry of the reactants (and hence host-rock chemistry).

For a particular host-rock chemistry (specifically Mg/Mg+Fe ratio), the lower-grade discontinuous reactions take place at a fixed temperature, and at fixed Mg/Mg+Fe ratios of the participating ferromagnesian phases (at a particular isotherm on the divariant loop of a T-X(Fe-Mg) diagram). With increasing temperature these Mg/Mg+Fe ratios remain unchanged through the biotite and cordierite zones. However, because different host-rock compositions define different Mg/Mg+Fe ratios in the ferromagnesian phases

at these reactions, the original variation in host-rock chemistry is reflected in a temperature-independent variation in the Mg/Mg+Fe ratio of biotite in these zones. Though these reactions do not cause changes in the Mg/Mg+Fe ratios of the phases, they can abruptly alter the Al/Mg+Fe ratio of a given reactant; i.e. muscovite becomes less phengitic at the biotite isograd, and biotite becomes more Al-rich at the cordierite isograd.

At higher grade, the incoming of cordierite + K-feldspar by the continuous reaction

$$\text{Biotite} + \text{Muscovite} + \text{Quartz} \rightarrow \text{Cordierite} + \text{K-feldspar} + H_2O$$

causes both the biotite and cordierite Mg/Mg+Fe ratios to shift toward more Fe-rich values along the divariant loop representing this reaction on the T-X(Fe-Mg) diagram. This is equivalent to a continuous shift of the three-phase AFM field biotite-cordierite-muscovite to more Fe-rich compositions. The Mg/Mg+Fe ratios are fixed ("frozen in"), however, at the temperature at which muscovite is exhausted. These Mg/Mg+Fe values remain fixed with increasing temperature unless the divariant loop representing the continuous reaction

$$\text{Biotite} + \text{Cordierite} + \text{Quartz} \rightarrow \text{Garnet} + \text{K-feldspar} + H_2O$$

is intersected. If intersected, this reaction causes a reversal in the Mg/Mg+Fe ratios of the ferromagnesian phases, shifting them to more Mg-rich values as temperature increases.

Discontinuous reactions, in the sense of Thompson (1976a), generated by the intersection of continuous reaction loops have not been recognised within the Walcha Road aureole, apparently because reactants are consumed on the divariant loops before this type of discontinuous reaction is reached.

Migmatites at the pluton contact appear from field morphology, textural and geochemical evidence, to have formed by partial melting of the pelites.

From a series of experimentally and theoretically based reactions, primarily on the stability of various cordierite-bearing assemblages, P-T conditions are estimated to range from between 350-400^{o}C at the outer edge of the aureole to 720-745^{o}C near the contact at pressures of 1-1½ Kb. Maximum pressures are delineated by the stability of cordierite + K-feldspar

before the breakdown of Muscovite + Quartz → Al-silicate + K-feldspar, requiring pressure to be below the invariant point PII in Fig. 3-9. Though the reactions defining the zone boundaries are dependent on composition, for the typical Mg/Mg+Fe ratios of the rocks studied in the Walcha Road aureole, the cordierite isograd is estimated at around 500-510^{o}C and the cordierite + K-feldspar zone boundary at about 560^{o}C. Insufficient data are available to accurately estimate the temperature of the biotite isograd. Similarly, P-T conditions cannot be accurately delineated for the garnet-forming reactions, however, garnet appears to be restricted to more Fe-rich (and probably more Mn-rich) rocks close to the contact, where temperatures in the vicinity of 720-745^{o}C are required to form the migmatites.